A Nonlinear Model Predictive Control for the Position Tracking of Cable-Driven Parallel Robots

João Cavalcanti Santos, Marc Gouttefarde, Ahmed Chemori

A Nonlinear Model Predictive Control for the Position Tracking of Cable-Driven Parallel Robots

João Cavalcanti Santos, Marc Gouttefarde, *Member, IEEE,* Ahmed Chemori, *Senior Member, IEEE*

***Abstract*—The present paper proposes a Nonlinear Model Predictive Control (NMPC) strategy for the position tracking of Cable-Driven Parallel Robots (CDPRs). The NMPC formulation handles explicitly the cable tensions and their limits. Accordingly, the cable tension distribution is performed as an integral part of the NMPC feedback control strategy, which notably allows the CDPR to operate on the wrench-feasible workspace boundaries without failure. In order to integrate the cable tension minimization within the NMPC formulation, the concept of Wrench Equivalent Optimality (WEO) is introduced. The WEO is a non-negative measure able to evaluate if the wrench generated by a given cable tension vector can be generated by an alternative tension vector with smaller 2-norm. The redundancy resolution performed by means of the minimization of the WEO enables the stability of the closed-loop system to be proved. More precisely, sufficient conditions for the uniform asymptotic stability are deduced using results from the analysis of NMPC schemes without terminal constraints and costs. Furthermore, the proposed NMPC strategy is validated experimentally on a fully-constrained 6 degree-of-freedom CDPR.**

***Index Terms*—Cable-Driven Parallel Robots, Model Predictive Control**

Nomenclature List

$\mathbb{S}^{n_s}$	Infinite sequences of vectors with length n_s
$\mathbb{S}^{n_{s1}}_{n_{s2}}$	Sequences of n_{s2} vectors with length n_{s1}
$\mathbb{U}$	Set of vectors of feasible cables tensions
$\mathbb{U}^{n_u}$	Sequences of n_u vectors of feasible cable tensions
$\mathbb{X}$	Set of admissible poses
$\mathbb{Y}$	Set of admissible states
$\mathbf{y}$	State vector
J_{hp}	$: \mathbb{N} \times \mathbb{Y} \times \mathbb{U}^{h_p} \to \mathbb{R}$, cost functional
ℓ	$: \mathbb{N} \times \mathbb{Y} \times \mathbb{U} \to \mathbb{R}$, stage cost
ℓ^*	$: \mathbb{N} \times \mathbb{Y} \to \mathbb{R}$, minimal time varying stage cost
$\boldsymbol{\phi}_{\mathbf{y}}$	$: \mathbb{Y} \times \mathbb{U} \to \mathbb{R}^{2n}$ transition mapping
$\boldsymbol{\tau}_{fb}$	$: \mathbb{N} \times \mathbb{Y} \to \mathbb{U}$, NMPC control policy
$\boldsymbol{\tau}_{wo}$	$: \mathbb{X} \times \mathbb{U} \to \mathbb{U}$, Wrench Equivalent optimal (WE-optimal) cable tensions
$\mathbf{y}_{\boldsymbol{\tau}(\cdot)}(\cdot, \mathbf{y}_a)$	$: \mathbb{N} \to \mathbb{R}^{2n}$, trajectory for initial state $\mathbf{y}_a$ and sequence of cable tensions $\boldsymbol{\tau}(\cdot)$
$\|\mathbf{v}\|_{\mathbf{K}}$,	weighted norm of a vector $\mathbf{v}$ given by $\sqrt{\mathbf{v}^T\mathbf{K}\mathbf{v}}$

The authors are with LIRMM, Univ Montpellier, CNRS, Montpellier, France e-mail: cavalcanti@lirmm.fr, gouttefarde@lirmm.fr and chemori@lirmm.fr

This work was supported by the European Union's H2020 Program (H2020/2014- 2020) under the grant agreement No. 732513 (HEPHAESTUS project). The authors also (greatly) acknowledge support of the European Union through FEDER grant n°49793.

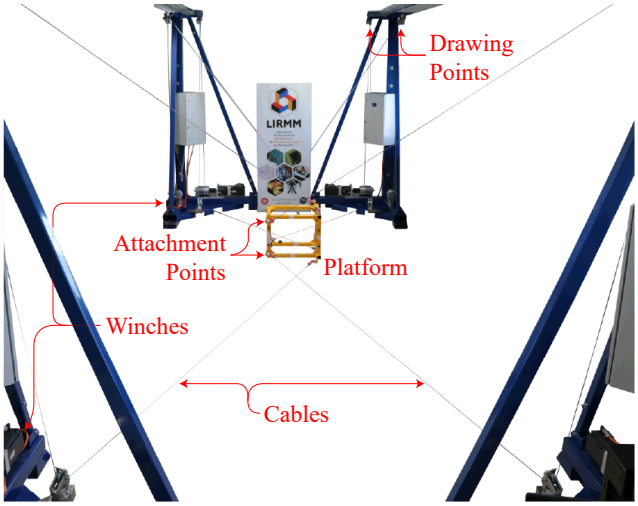

Fig. 1. HRPCable prototype, a 6-DoF fully-constrained CDPR.

I. Introduction

POSITION tracking control of Cable-Driven Parallel Robots (CDPRs) addresses the problem of generating a mobile platform trajectory as close as possible to a desired one. The majority of previous works dealing with this problem implemented model-based strategies including a feedforward input based on the system dynamics [1]–[18]. Acceptable results can notably be obtained with a PID feedback correction combined to computed torque control [1]–[5] or with a similar approach with position-controlled winches [6]. Nevertheless, advanced control techniques may lead to improved results. Sliding Mode Control (SMC) [19] received particular attention in this context [9]–[14]. SMC is well-known to present easy implementation, good robustness against modeling uncertainties and, generally, finite time convergence. Babaghasabha *et al.* [9] applied this control strategy to a planar CDPR. Terminal sliding mode [10] and super twisting controller [11] are improved versions of SMC that were used to control CDPRs. Some other examples of advanced control techniques used with the same goal are $\mathscr{H}_\infty$ [15], [16], Lyapunov-based controllers [17], [18] , and learning-based tracking controllers [20].

Although minimum and maximum cable tension limits play a crucial role in the operation of a CDPR, the control strategies proposed in [1]–[18] are not able to handle these constraints as an integral part of the feedback motion controller. These constraints are typically handled in a *cable tension distribution* algorithm, *e.g.* [21]–[26], which takes place once the desired wrench is already computed by the controller. As

a consequence, an unfeasible desired wrench taken as the input to a tension distribution algorithm generally leads to a control breakdown. This kind of feasibility issue typically arises close to the boundaries of the CDPR wrench-feasible workspace (WFW) [27] or in presence of significant modeling uncertainties or disturbances.

To overcome this problem, a Model Predictive Control (MPC) strategy was introduced in our preliminary work [28]. As highlighted in [29], MPC is one of the few control strategies able to handle system constraints explicitly. Thus, the Linear MPC (LMPC) introduced in [28] integrates the cable tension distribution calculation within its formulation. Experimental results showed that this MPC is not prone to the aforementioned feasibility issues since it can operate on the WFW boundary without failure.

In spite of the significant improvements obtained in [28], the stability analysis of the corresponding closed-loop system is hindered by the linear approximation of the actual CDPR nonlinear dynamics. Furthermore, the obtained tracking error leaves room for improvement. In this context, the Nonlinear Model Predictive Control (NMPC) strategy introduced in the present paper seeks to ally superior tracking precision and a closed-loop stability proof, in addition to the aforementioned ability to work on the WFW boundary without failure.

Apart from [28], studies addressing MPC schemes for CDPRs are very few [30], [31]. Katliar *et al.* proposed in [30] an NMPC to generate a desired set of accelerations and velocities for a motion simulator. Its performance was investigated through numerical simulations while the closed-loop system stability and the ability to work close to the WFW boundaries were not addressed. Moreover, the present paper deals with trajectory tracking and prioritizes positioning accuracy. Numerical simulations and experimental results are presented in [31]. However, the proposed LMPC is meant for vibration attenuation of a 2-DoF planar CDPR where only some of the cables are controlled in tension and the closed-loop system stability is not addressed. The NMPC proposed in the present paper is compatible with any CDPR actuated by at least as many cables as number of DoFs. Experimental validation is done on a 6-DoF CDPR whose eight cable tensions are controlled by the NMPC scheme in real time. Additionally, the focus of the present work is position tracking control, instead of vibration attenuation.

Regarding the stability of systems controlled with MPC schemes, [32] advocates that terminal costs and constraints (shortly referred to as terminal conditions) represent a powerful tool since the stability of the closed-loop system is deduced as a direct consequence of Lyapunov stability theory [33, Section 2.4]. Accordingly, numerous applications of MPC in robotics used terminal conditions [34]–[39]. Nevertheless, the use of terminal conditions in an MPC scheme may lead to important drawbacks such as terminal constraint construction issues, increased computational burden, and operating range limitations [40]. More specifically, terminal constraints may render an MPC scheme more prone to unfeasible optimization problems in particular when operating close to system constraints, which goes against the ability to work close to the WFW boundary without failure such as demonstrated in [28]. Advantages and drawbacks of terminal conditions are further discussed in [41], [42] and [43, Section 7.4].

Alternatively, MPC schemes without terminal conditions can be used. The formulation and real-time solution of the corresponding optimization problems without additional constraints are simplified. However, more advanced techniques are necessary in order to guarantee the stability of the closed-loop system since it cannot be deduced as a direct consequence of Lyapunov stability theory. Hence, several studies used MPC schemes without terminal conditions in robotics [31], [44]–[49], but very few performed a stability analysis, e.g., Worthmann *et al.* [50] use a non-quadratic stage cost for the NMPC without terminal conditions of non-holonomic mobile robots and attain a stable closed-loop system. Position tracking control of CDPRs presents paramount differences with the steering of non-holonomic mobile robots so that the results obtained in [50] are not applicable in the present paper. Nevertheless, similarly to [50], the proposed NMPC scheme stability analysis will be based on [43, Chapter 6].

In order to apply the theory of Grüne and Pannek [43], the NMPC scheme proposed in this paper applies an original formulation of the cost functional. Many MPC applications in robotics use the penalization of (i) the tracking errors, (ii) the amplitude of the control inputs and/or (iii) the variation of the control inputs. Typically, the corresponding cost function consists of one of these three variables or of a weighted sum of two of them [37], [44], [45], [47]–[49]. Indeed, this was the case for the above mentioned MPC schemes used to control CDPRs [28], [30], [31], in which the cable tensions were taken as the control inputs. However, for the position tracking control of CDPRs, this formulation is not consistent with the methodology used for the stability analysis of NMPC schemes presented in [43, Chapter 6] and may lead to deteriorated tracking errors. Indeed, an NMPC scheme considering (ii) and/or (iii) is generally not able to track a feasible desired trajectory with null tracking errors since the optimization of a cost functional consisting of a weighted sum of (i)-(iii) leads to a compromise between these three aspects, which generally have different individual minima. In other words, the minimization of a weighted sum of (i)-(iii) seeks to minimize (ii) and/or (iii) to the detriment of (i), the tracking error. The control scheme proposed in this work provides a solution to this issue.

The main contribution of the present paper is the formulation of an NMPC scheme for the position tracking control of CDPRs using the concept of Wrench Equivalent Optimality (WEO). For a given platform pose and a set of cable tensions, the WEO is a non-negative measure that evaluates whether the wrench generated by these cable tensions can be generated by an alternative cable tension vector with smaller 2-norm. The penalization of the WEO is consistent with the minimization of the tracking errors in the sense that both tracking errors and WEO can be null. By means of this original formulation, the cable tension distribution is implicitly performed in real time and the stability of the closed-loop system is analyzed using methods for the analysis of NMPC schemes without terminal conditions. In addition, since the cable tensions are explicitly handled in the NMPC controller, the proposed strategy allows

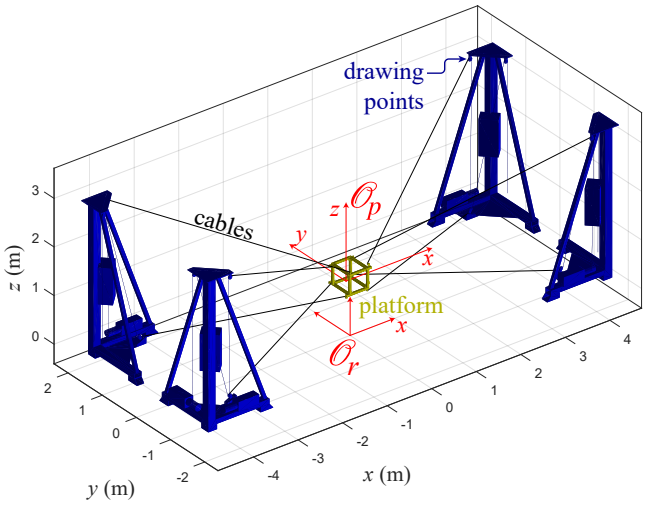

Fig. 2. CAD view of the HRPCable prototype.

the CDPR to operate on the boundary of the WFW without failure. Finally, compared to the state-of-the-art LMPC scheme [28], the proposed strategy leads to improved tracking errors.

The tracking error improvement is validated experimentally on a 6-DoF CDPR whose mobile platform follows a typical pick-and-place trajectory. In these experiments, in order to show that the proposed scheme can operate on the WFW boundary without failing, the same pick-and-place path is performed with maximum allowed tensions drastically reduced. The desired trajectory escapes from the WFW defined with these new cable tension limits. The proposed NMPC is able to track a trajectory as close as possible to the desired one without violating the cable tension limits, some tensions attaining their maximum limit. In order to highlight the relevance of this feature, the same trajectory is performed with the control scheme proposed in [5]. In this case, as soon as the desired trajectory reaches an unfeasible pose, the CDPR operation is terminated because the controller requires the tension distribution module to generate an unfeasible wrench. Note that this infeasibility issue would also be obtained with advanced control schemes such as robust [2], [3] and adaptive [9]–[11] strategies.

This paper is organized as follows. Section II presents the CDPR continuous and discrete-time dynamic models. Section III introduces the proposed NMPC scheme. In Section IV, the stability of the corresponding closed-loop system is analyzed. In Section V, the proposed NMPC scheme is compared to an LMPC in numerical simulations. Experimental results are presented in Section VI and conclusions are drawn in Section VII. Appendices A, B and C discuss some details on the dynamic model and on the stability analysis. Appendix D briefly describes the used numerical optimization methods.

II. Preliminaries and Dynamic Models

This section presents the continuous dynamic model of a CDPR consisting of an n-DoF mobile platform driven by m cables, where $n \leqslant m$. An example of a 6-DoF CDPR driven by 8 cables is depicted in Figure 2. As for most of the typical applications of MPC in robotics, the control scheme proposed in Section III is based on a discrete-time system. Accordingly, a discrete-time CDPR dynamic model based on its continuous counterpart is also presented.

The platform pose is given by the vector-valued function $\boldsymbol{x}:\mathbb{R}\rightarrow\mathbb{R}^n$, so that $\boldsymbol{x}(t)=\begin{bmatrix}\boldsymbol{p}(t)^T & \boldsymbol{\psi}(t)^T\end{bmatrix}^T$ is the pose vector containing both the platform position $\boldsymbol{p}(t)$ and orientation $\boldsymbol{\psi}(t)$ at instant t. These vectors are written with respect to the fixed reference frame $\mathscr{O}_r$, as depicted Figure 2. Typically, $\boldsymbol{\psi}(t)$ consists of Euler angles. The dependence on time is dropped leading to the shorthand notation $\boldsymbol{x}$ whenever there is no risk of confusion. The same shorthand notation is used for other vector-valued and matrix-valued functions in the remainder of this paper. The common dot notation is used to refer to the time derivatives, so that $\mathrm{d}\boldsymbol{x}/\mathrm{dt}=\dot{\boldsymbol{x}}$ and $\mathrm{d}^2\boldsymbol{x}/\mathrm{dt}^2=\ddot{\boldsymbol{x}}$.

The vector-valued function $\boldsymbol{\tau}_c:\mathbb{R}\rightarrow\mathbb{R}^m$ represents the vector of cable tensions in function of time $\boldsymbol{\tau}_c(t)=\begin{bmatrix}\tau_1(t) & \dots & \tau_m(t)\end{bmatrix}^T$. Each cable force is applied on the corresponding attachment point of the mobile platform (see Figure 1). The mobile platform equations of motion can be obtained with the Newton-Euler formalism, which, neglecting cable distributed mass, leads to the following dynamic model

$$\mathbf{M}(\boldsymbol{x})\,\ddot{\boldsymbol{x}}+\mathbf{C}(\boldsymbol{x},\dot{\boldsymbol{x}})\,\dot{\boldsymbol{x}}=\mathbf{g}(\boldsymbol{x})+\mathbf{W}(\boldsymbol{x})\,\boldsymbol{\tau}_c, \tag{1}$$

where $\mathbf{M}(\boldsymbol{x})$ is the mass matrix, $\mathbf{C}(\boldsymbol{x},\dot{\boldsymbol{x}})$ is the vector of Coriolis and centripetal forces, $\mathbf{g}(\boldsymbol{x})$ is the vector of gravitational forces and $\mathbf{W}(\boldsymbol{x})$ is the wrench matrix. Details on the continuous dynamic model (1) are discussed in Appendix A.

Based on the nonlinear continuous-time system (1), it is necessary to define the discrete-time dynamic model that will be used in Section III. This discrete-time model is written in terms of sequences of vectors, which are denoted with bold (non-italic) lowercase letters followed by $(\cdot)$ (such as, for instance, $\mathbf{s}(\cdot)$). The set of sequences of vectors with dimension n_s and infinite number of elements is denoted as $\mathbb{S}^{n_s}$. More precisely,

$$\mathbb{S}^{n_s}=\{\mathbf{s}(\cdot):\mathbb{N}_0\rightarrow\mathbb{R}^{n_s}\}, \tag{2}$$

with $\mathbb{N}_0=\mathbb{N}\cup\{0\}$ the set of non-negative integers and $\mathbb{N}$ the set of strictly positive integers. Accordingly, the k^{th} vector of a sequence $\mathbf{s}(\cdot)\in\mathbb{S}^{n_s}$ is denoted as $\mathbf{s}(k)=\mathbf{s}_k\in\mathbb{R}^{n_s}$.

Consider the sequences of vectors $\mathbf{x}(\cdot)$, $\dot{\mathbf{x}}(\cdot)$, $\ddot{\mathbf{x}}(\cdot)\in\mathbb{S}^n$ and $\mathbf{y}(\cdot)\in\mathbb{S}^{2n}$ defined as

$$\begin{aligned}\mathbf{x}(k)&=\mathbf{x}_k=\boldsymbol{x}(t_0+k\Delta t)\\ \dot{\mathbf{x}}(k)&=\dot{\mathbf{x}}_k=\dot{\boldsymbol{x}}(t_0+k\Delta t)\\ \ddot{\mathbf{x}}(k)&=\ddot{\mathbf{x}}_k=\ddot{\boldsymbol{x}}(t_0+k\Delta t)\\ \mathbf{y}(k)&=\mathbf{y}_k=\begin{bmatrix}\mathbf{x}_k^T & \dot{\mathbf{x}}_k^T\end{bmatrix}^T\end{aligned} \tag{3}$$

for all $k\in\mathbb{N}_0$, an initial time t_0 and a sampling period Δt. Without loss of generality, since the continuous system (1) is time-invariant (according to the definition in [51, Chapter 1]) the initial time is considered to be $t_0=0$. The subsequent time instants are denoted as $t_1=\Delta t$, $t_2=2\Delta t,\dots$, $t_k=k\Delta t$, for $k\in\mathbb{N}_0$.

Similarly, considering a digital control approach, the continuous-time representation $\boldsymbol{\tau}_c$ of the actual cable tensions

is considered piece-wise constant and given by its discrete counterpart $\boldsymbol{\tau}(\cdot) \in \mathbb{S}^m$, *i.e.*:

$$\boldsymbol{\tau}(k) = \boldsymbol{\tau}_k = \boldsymbol{\tau}_c(t), \text{ for } k\Delta t < t \leqslant (k+1)\Delta t \text{ and } k \in \mathbb{N}_0. \quad (4)$$

Typically, every cable tension vector $\boldsymbol{\tau}_k, \forall k \in \mathbb{N}_0$ should satisfy $\boldsymbol{\tau}_{min} \leqslant \boldsymbol{\tau}_k \leqslant \boldsymbol{\tau}_{max}$, for constant $\boldsymbol{\tau}_{min}$, $\boldsymbol{\tau}_{max} \in \mathbb{R}^m_+$ and $\mathbb{R}^m_+ = \{\mathbf{v} \in \mathbb{R}^m | \, \mathbf{v} > 0\}$. The set of admissible cable tensions $\mathbb{U} \subset \mathbb{R}^m_+$ is thus defined as

$$\mathbb{U} = \{\boldsymbol{\tau} \in \mathbb{R}^m \mid \mathbf{0} < \boldsymbol{\tau}_{min} \leqslant \boldsymbol{\tau} \leqslant \boldsymbol{\tau}_{max}\}. \quad (5)$$

Consider a sequence of feasible cable tensions $\boldsymbol{\tau}(\cdot) \in \mathbb{S}^m$ represented by an infinite number of vectors $\{\boldsymbol{\tau}_0, \boldsymbol{\tau}_1, \dots\}$. For a given time instant $k \in \mathbb{N}_0$, special attention will be devoted to the finite sequence of cable tensions $\{\boldsymbol{\tau}_k, \boldsymbol{\tau}_{k+1}, \dots, \boldsymbol{\tau}_{k+h_p-1}\}$, with a positive integer h_p. Accordingly, the following set of truncated sequences with a finite number of feasible cable tension vectors is introduced:

$$\mathbb{U}_k^{h_p} = \left\{ \boldsymbol{\tau}(\cdot) : \mathbb{N}_{k,k+h_p-1} \to \mathbb{U} \right\}, \quad (6)$$

where, $\mathbb{N}_{n_1,n_2} = \{i \in \mathbb{N}_0 | \, n_1 \leqslant i \leqslant n_2\}$, for given $n_1, n_2 \in \mathbb{N}_0$.

In order to define a discrete-time dynamic model based on (1), variables $\mathbf{x}_{k+1}$ and $\dot{\mathbf{x}}_{k+1}$ should be computed based on known $\mathbf{x}_k$, $\dot{\mathbf{x}}_k$ and $\boldsymbol{\tau}_k$. The following discrete-time dynamic system is considered:

$$\mathbf{y}_{k+1} = \overbrace{\begin{bmatrix} \mathbf{I} & \Delta t\, \mathbf{I} \\ \mathbf{0} & \mathbf{I} \end{bmatrix}}^{\mathbf{A}} \mathbf{y}_k + \overbrace{\begin{bmatrix} \mathbf{0} \\ \Delta t\, \mathbf{M}(\mathbf{x}_k)^{-1}\, \mathbf{W}(\mathbf{x}_k) \end{bmatrix}}^{\mathbf{B}(\mathbf{y}_k)} \boldsymbol{\tau}_k + \underbrace{\begin{bmatrix} \mathbf{0} \\ \Delta t\, \mathbf{M}(\mathbf{x}_{\mathbf{y}_k})^{-1} \big(\mathbf{g}(\mathbf{x}_k) - \mathbf{C}(\mathbf{x}_k, \dot{\mathbf{x}}_k)\dot{\mathbf{x}}_k\big) \end{bmatrix}}_{\mathbf{v}(\mathbf{y}_k)} \quad (7)$$

or, using a more compact notation,

$$\mathbf{y}_{k+1} = \boldsymbol{\phi}_{\mathbf{y}}(\mathbf{y}_k, \boldsymbol{\tau}_k) = \mathbf{A}\,\mathbf{y}_k + \mathbf{B}(\mathbf{y}_k)\,\boldsymbol{\tau}_k + \mathbf{v}(\mathbf{y}_k) \quad (8)$$

with $\boldsymbol{\phi}_{\mathbf{y}}(\mathbf{y}_k, \boldsymbol{\tau}_k)$ denoting the transition mapping that represents the discrete-time dynamic model. Details on the deduction of this model are given in Appendix A.

The transition mapping in (8) can be used in the prediction step of an NMPC scheme. For a state $\mathbf{y}_k \in \mathbb{R}^{2n}$, the sequence of $h_p \in \mathbb{N}$ future states is predicted for a known sequence of future cable tensions $\boldsymbol{\tau}(\cdot) \in \mathbb{U}_k^{h_p}$ by using the transition mapping $\boldsymbol{\phi}_{\mathbf{y}}$ recursively. More precisely,

$$\begin{aligned} \mathbf{y}_{\boldsymbol{\tau}(\cdot)}(0, \mathbf{y}_k) &= \mathbf{y}_k \\ \mathbf{y}_{k+1} = \mathbf{y}_{\boldsymbol{\tau}(\cdot)}(1, \mathbf{y}_k) &= \boldsymbol{\phi}_{\mathbf{y}}(\mathbf{y}_k, \boldsymbol{\tau}_k) \\ \mathbf{y}_{k+2} = \mathbf{y}_{\boldsymbol{\tau}(\cdot)}(2, \mathbf{y}_k) &= \boldsymbol{\phi}_{\mathbf{y}}(\mathbf{y}_{k+1}, \boldsymbol{\tau}_{k+1}) \\ &\vdots \\ \mathbf{y}_{k+h_p} = \mathbf{y}_{\boldsymbol{\tau}(\cdot)}(h_p, \mathbf{y}_k) &= \boldsymbol{\phi}_{\mathbf{y}}\left(\mathbf{y}_{k+h_p-1}, \boldsymbol{\tau}_{k+h_p-1}\right) \end{aligned} \quad (9)$$

where the state $\mathbf{y}_{\boldsymbol{\tau}(\cdot)}(j, \mathbf{y}_k)$ represents the j^{th} term of the sequence of predicted future states $\mathbf{y}_{\boldsymbol{\tau}(\cdot)}(\cdot, \mathbf{y}_k)$ resulting from the application of the cable tensions $\boldsymbol{\tau}(\cdot) \in \mathbb{U}_k^{h_p}$ taking as initial state $\mathbf{y}_k$. The strictly positive integer h_p is called *prediction horizon*.

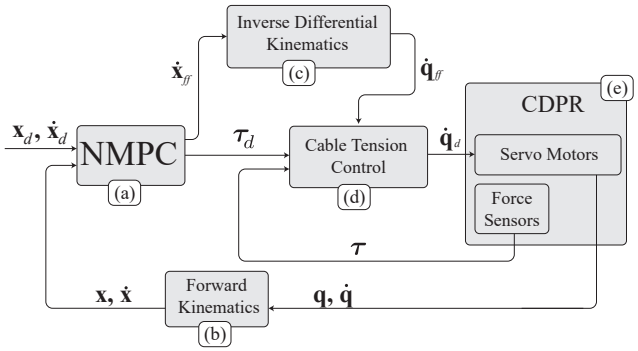

Fig. 3. Block diagram of a position tracking control scheme integrating the proposed NMPC.

Although the domain of $\boldsymbol{\phi}_{\mathbf{y}}$ may be defined as $\mathbb{R}^{2n} \times \mathbb{R}^m$, a proper CDPR operation should be constrained to a limited set of cable tensions. For this reason, the set of feasible cable tensions $\mathbb{U}$ is used instead of $\mathbb{R}^m$. Similarly, a constrained set of platform poses and velocities should be defined. The set $\mathbb{Y} \subset \mathbb{R}^{2n}$ is thus defined as the set of all admissible states $\mathbf{y} \in \mathbb{R}^{2n}$ within which the controller is able to operate. The definition of $\mathbb{Y}$ should use tools related to the computation of the workspace of CDPRs, *e.g.* [52]–[56]. More details on this matter are discussed in Section VI-A2. The set $\mathbb{X} \subset \mathbb{R}^n$ is defined as the projection of the set $\mathbb{Y}$ on the space of platform poses, *i.e.* $\mathbb{X} = \{\mathbf{x} \in \mathbb{R}^n \mid \exists\ \dot{\mathbf{x}} \in \mathbb{R}^n \ : \ \begin{bmatrix} \mathbf{x}^T & \dot{\mathbf{x}}^T \end{bmatrix}^T \in \mathbb{Y}\}$. In summary, the domain of $\boldsymbol{\phi}_{\mathbf{y}}$ is defined as $\mathbb{Y} \times \mathbb{U}$.

III. NMPC FOR CDPR POSITION TRACKING

The block diagram in Figure 3 outlines an overall position tracking control scheme integrating the NMPC strategy proposed in this paper. Based on the desired and estimated platform motions ($\mathbf{x}_d(\cdot)$, $\dot{\mathbf{x}}_d(\cdot) \in \mathbb{S}^n$ and $\mathbf{x}(\cdot)$, $\dot{\mathbf{x}}(\cdot) \in \mathbb{S}^n$, respectively), the NMPC scheme (block (a)) defines a set of desired cable tensions $\boldsymbol{\tau}_d(\cdot) \in \mathbb{S}^m$. The cable tension control in block (d) is responsible for generating these cable tensions by means of desired motor velocities $\dot{\mathbf{q}}_d$. As described in [28] and [57], $\dot{\mathbf{q}}_d$ is computed applying a feedforward term $\dot{\mathbf{q}}_{ff}$ related to the platform velocity in addition to a PI feedback correction based on the error between the actual cable tensions and the desired ones. In addition, the authors showed in [57] that this simple non model-based control scheme leads to small tension tracking errors even in the presence of friction. The actual platform pose and velocity are estimated based on the measured motor positions and velocities. Blocks (b) and (c) correspond to the kinematic modeling of the CDPR and can be implemented using well-known methods, *e.g.* [58]–[60]. Note that the NMPC in block (a) is independent of blocks (b), (c) and (d) and thus independent of cable properties (*e.g.* elasticity) and friction at the winches and routing pulleys.

The predicted platform velocity $\dot{\mathbf{x}}_{ff}$ is obtained within the NMPC block applying (8) with $\boldsymbol{\tau}_d(k)$.

The NMPC scheme introduced in this section is consistent with the standard formulation of NMPC schemes without terminal conditions [43]. In accordance with the definition of receding horizon MPC schemes [32], the proposed NMPC

strategy solves an Optimal Control Problem (OCP) at each controller cycle such that a cost functional is minimized while satisfying system constraints. Since no terminal condition is used, the cost functional, denoted by $J_{h_p} : \mathbb{N}_0 \times \mathbb{Y} \times \mathbb{U}_k^{h_p} \to \mathbb{R}$ for a given $k \in \mathbb{N}_0$, consists of a sum of individual costs associated to each sampling time within the prediction horizon $h_p \in \mathbb{N}$. The function that computes these individual costs is called *stage cost* and is denoted by $\ell : \mathbb{N}_0 \times \mathbb{Y} \times \mathbb{U} \to \mathbb{R}$. Therefore, for an instant $k \in \mathbb{N}_0$, actual state $\mathbf{y}_k \in \mathbb{Y}$ and sequence of cable tensions $\boldsymbol{\tau}(\cdot) \in \mathbb{U}_k^{h_p}$, the cost functional is given by

$$J_{h_p}(k, \mathbf{y}_k, \boldsymbol{\tau}(\cdot)) = \sum_{j=0}^{h_p-1} \ell\left(k+j, \mathbf{y}_{\boldsymbol{\tau}(\cdot)}(j, \mathbf{y}_k), \boldsymbol{\tau}_{k+j}\right). \tag{10}$$

Algorithm 1 summarizes the common implementation of NMPC schemes without terminal conditions applying the notations used in this paper. Algorithm 1-(b) defines the control policy $\boldsymbol{\tau}_{fb} : \mathbb{N}_0 \times \mathbb{Y} \to \mathbb{U}$, which computes the vector of desired cable tensions $\boldsymbol{\tau}_{fb}(k, \mathbf{y}_k)$ at instant $k \in \mathbb{N}_0$ and for state $\mathbf{y}_k \in \mathbb{Y}$. This vector is computed based on the minimization of the cost functional J_{h_p}. The computation of J_{h_p} applies the discrete-time system (8) in order to predict the h_p future states, as in (9). The cost functional J_{h_p} is computed considering a given stage cost ℓ (which will be defined later in this section). The control policy $\boldsymbol{\tau}_{fb}$ is used in Algorithm 1-(a) such that the minimization of J_{h_p} is solved at each controller cycle with updated estimations of the states. As main output, the NMPC scheme defines a set of desired cable tensions $\boldsymbol{\tau}_d(k)$ to be applied in the time interval $t \in [k\Delta t,\ (k+1)\Delta t)$. These outputs are used as setpoints for the cable tension control in block (d) shown in Figure 3. The numerical procedure used for the minimization of J_{h_p} is discussed in Appendix D.

The definition of a pertinent stage cost is a crucial step in the design of a stable and effective NMPC scheme. In order to meet the theoretical requirements necessary to guarantee stability and obtain appropriate performances, one should seek some particular properties of the stage cost. Postponing the formal developments on this matter to Section IV, some key properties are sketched in the next paragraphs to explain the rationale used in the design of the proposed OCP.

Typically, NMPC schemes penalize states and control inputs with respect to the *desired behavior of the system*. The following definition rigorously formulates such desired behavior.

Definition 1. *Consider the sequences $\mathbf{x}_d(\cdot), \dot{\mathbf{x}}_d(\cdot) \in \mathbb{S}^n$ of desired poses and velocities, respectively, and $\mathbf{y}_d(\cdot) \in \mathbb{S}^{2n}$, with $\mathbf{y}_d(k) = \begin{bmatrix}\mathbf{x}_d(k)^T & \dot{\mathbf{x}}_d(k)^T\end{bmatrix}^T$, the desired trajectory. The sequence $\mathbf{y}_d(\cdot)$ is called **feasible** if there exists a sequence of nominal desired cable tensions $\boldsymbol{\tau}_{nd}(\cdot) \in \mathbb{S}^m$ such that, for $\mathbf{y}_0 = \mathbf{y}_d(0)$,*

$$\mathbf{y}_{\boldsymbol{\tau}_{nd}(\cdot)}(k, \mathbf{y}_0) = \mathbf{y}_d(k) \in \mathbb{Y} \text{ and } \boldsymbol{\tau}_{nd}(k) \in \mathbb{U} \tag{11}$$

for all $k \in \mathbb{N}$. Moreover, each vector of $\boldsymbol{\tau}_{nd}(\cdot)$ is considered to have minimal 2-norm such that, for every $k \in \mathbb{N}$,

$$\nexists\ \boldsymbol{\tau} \in \mathbb{U} \mid \mathbf{W}(\mathbf{x}_d(k))\,\boldsymbol{\tau}_{nd}(k) = \mathbf{W}(\mathbf{x}_d(k))\,\boldsymbol{\tau} \text{ and } \|\boldsymbol{\tau}\| < \|\boldsymbol{\tau}_{nd}(k)\|. \tag{12}$$

Algorithm 1 NMPC Algorithm

(a) Overall NMPC Implementation

1: Set $k \leftarrow 0$;
2: **loop**
3: Estimate the actual states $\mathbf{y}_k$ using a forward kinematic model;
4: Set desired cable tensions $\boldsymbol{\tau}_d(k) \leftarrow \boldsymbol{\tau}_{fb}(k, \mathbf{y}_k)$ valid for $t \in [k\Delta t,\ (k+1)\Delta t)$;
5: Set $k \leftarrow k+1$;
6: **end loop**

(b) Control policy - computation of the desired cable tensions

Inputs: $\begin{bmatrix}\mathbf{x}_k^T & \dot{\mathbf{x}}_k^T\end{bmatrix}^T = \mathbf{y}_k \in \mathbb{Y}$ and $k \in \mathbb{N}_0$;
Output: $\boldsymbol{\tau}_{fb} \in \mathbb{U}$;

1: **function** $\boldsymbol{\tau}_{fb}(k, \mathbf{y}_k)$
2: Find $\boldsymbol{\tau}^*(\cdot) \in \mathbb{U}_k^{h_p}$ that minimizes $J_{h_p}\left(k, \mathbf{y}_k, \boldsymbol{\tau}(\cdot)\right)$ and satisfies constraints (16b);
3: Set $\boldsymbol{\tau}_{fb} \leftarrow \boldsymbol{\tau}_k^* = \boldsymbol{\tau}^*(k)$;
4: **return** $\boldsymbol{\tau}_{fb}$.
5: **end function**

*A desired trajectory $\mathbf{y}_d(\cdot) \in \mathbb{S}^{2n}$ that does not satisfy the aforementioned conditions is called **unfeasible**.*

As indicated in (12) each vector of $\boldsymbol{\tau}_{nd}(\cdot)$ presents minimal 2-norm. Indeed, the minimization of the 2-norm of the vector of cable tensions is widely used in the state-of-the-art control schemes, *e.g.* [22]–[24]. This choice leads to continuous cable tension while minimizing the energy consumption [23].

The cost functional of a typical NMPC scheme should be null for state and cable tensions equal to the desired trajectory and nominal desired cable tensions, respectively, and strictly positive if the state is not equal to the desired one. More precisely, the stage cost function should satisfy (see [43, Section 3.3])

$$\begin{cases} \ell(k, \mathbf{y}, \boldsymbol{\tau}) = 0 \text{ if } \mathbf{y} = \mathbf{y}_d(k) \text{ and } \boldsymbol{\tau} = \boldsymbol{\tau}_{nd}(k), \\ \ell(k, \mathbf{y}, \boldsymbol{\tau}) > 0 \text{ if } \mathbf{y} \neq \mathbf{y}_d(k). \end{cases} \tag{13}$$

Aiming at a stage cost satisfying (13), $\ell(k, \mathbf{y}, \boldsymbol{\tau})$ could be defined as a sum of weighted norms such as $\|\mathbf{y} - \mathbf{y}_d(k)\|_{\mathbf{K}_\mathbf{y}} + \|\boldsymbol{\tau} - \boldsymbol{\tau}_{nd}(k)\|_{\mathbf{K}_{\boldsymbol{\tau}}}$, with $\|\mathbf{v}\|_\mathbf{K} = \sqrt{\mathbf{v}^T \mathbf{K} \mathbf{v}}$, for any vector $\mathbf{v}$ and positive definite matrix $\mathbf{K}$. Nevertheless, in order to obtain $\boldsymbol{\tau}_{nd}(\cdot)$, one would need to solve the tension distribution problem along the whole trajectory beforehand, using a tension distribution algorithm. The nominal wrenches to be applied on the platform should then be computed based on the nominal inverse dynamics. Therefore, these wrenches could not be updated in the controller real-time operation. Due to the incidence of disturbances and modeling uncertainties, the wrench computed with the nominal inverse dynamics can be inefficient for the tracking control. Furthermore, the desired trajectory should be feasible in the sense that there exists a

sequence of cable tension distributions in $\mathbb{U}$ able to generate this trajectory.

Conversely, the proposed NMPC scheme is able to define in real time the optimal cable tension distribution without fixing a desired wrench. For this purpose, the following stage cost is proposed:

$$\ell(k,\mathbf{y},\boldsymbol{\tau}) = \|\mathbf{y}-\mathbf{y}_d(k)\|^2_{\mathbf{K_y}} + \|\boldsymbol{\tau}-\boldsymbol{\tau}_{wo}(\mathbf{x_y},\boldsymbol{\tau})\|^2_{\mathbf{K}_{\boldsymbol{\tau}}}, \tag{14}$$

where $\mathbf{K_y} = \mathrm{diag}(\mathbf{k_y})$ and $\mathbf{K}_{\boldsymbol{\tau}} = \mathrm{diag}(\mathbf{k}_{\boldsymbol{\tau}})$, with constant weighting vectors $\mathbf{k_y} \in \mathbb{R}^{2n}_+$ and $\mathbf{k}_{\boldsymbol{\tau}} \in \mathbb{R}^m_+$. The term $\|\boldsymbol{\tau}-\boldsymbol{\tau}_{wo}(\mathbf{x_y},\boldsymbol{\tau})\|^2_{\mathbf{K}_{\boldsymbol{\tau}}}$ represents the Wrench Equivalent Optimality (WEO) with respect to $\mathbf{x_y}$ and $\boldsymbol{\tau}$. The WEO is a non-negative measure that evaluates whether the wrench generated by $\boldsymbol{\tau}$ can be generated by an alternative set of cable tensions with smaller 2-norm at the pose $\mathbf{x_y}$. More precisely, for given $\mathbf{x} \in \mathbb{X}$ and $\boldsymbol{\tau} \in \mathbb{U}$, the vector-valued function $\boldsymbol{\tau}_{wo} : \mathbb{X} \times \mathbb{U} \to \mathbb{U}$ denotes the *wrench equivalent optimal* (WE-optimal) cable tensions, defined as

$$\boldsymbol{\tau}_{wo}(\mathbf{x},\boldsymbol{\tau}) = \arg\min_{\boldsymbol{\tau}'} \ \|\boldsymbol{\tau}'\|^2 \tag{15a}$$

$$\text{s.t. } \mathbf{W}(\mathbf{x})\,\boldsymbol{\tau} = \mathbf{W}(\mathbf{x})\,\boldsymbol{\tau}' \tag{15b}$$

$$\boldsymbol{\tau}_{min} \leqslant \boldsymbol{\tau}' \leqslant \boldsymbol{\tau}_{max} \tag{15c}$$

In words, $\boldsymbol{\tau}_{wo}(\mathbf{x},\boldsymbol{\tau})$ is the vector of cable tensions with minimal 2-norm that is able to generate the same wrench as $\boldsymbol{\tau}$ at the pose $\mathbf{x}$. Therefore, for given $k \in \mathbb{N}$, $\mathbf{y} \in \mathbb{Y}$ and $\boldsymbol{\tau} \in \mathbb{U}$, the term $\|\boldsymbol{\tau}-\boldsymbol{\tau}_{wo}(\mathbf{x_y},\boldsymbol{\tau})\|^2_{\mathbf{K}_{\boldsymbol{\tau}}} = 0$ iff $\boldsymbol{\tau}$ has minimal 2-norm ($\boldsymbol{\tau} = \boldsymbol{\tau}_{wo}(\mathbf{x_y},\boldsymbol{\tau})$). Otherwise, $\|\boldsymbol{\tau}-\boldsymbol{\tau}_{wo}(\mathbf{x_y},\boldsymbol{\tau})\|^2_{\mathbf{K}_{\boldsymbol{\tau}}} > 0$, indicating that there exists a $\boldsymbol{\tau}_{wo}(\mathbf{x_y},\boldsymbol{\tau}) \in \mathbb{U}$ generating the same wrench (thanks to (15b)) with $\|\boldsymbol{\tau}_{wo}(\mathbf{x_y},\boldsymbol{\tau})\| < \|\boldsymbol{\tau}\|$.

Accordingly, for given time instant $k \in \mathbb{N}_0$ and state $\mathbf{y}_k \in \mathbb{Y}$, the OCP solved in Algorithm 1-(b), which corresponds to the minimization of $J_{h_p}(k,\mathbf{y}_k,\boldsymbol{\tau}(\cdot))$ with respect to $\boldsymbol{\tau}(\cdot)$, can be written as

$$\min_{\boldsymbol{\tau}(\cdot)\in\mathbb{U}_k^{h_p}} \ \sum_{j=0}^{h_p-1} \ell\big(k+j, \mathbf{y}_{\boldsymbol{\tau}(\cdot)}(j,\mathbf{y}_k), \boldsymbol{\tau}_{k+j}\big) \tag{16a}$$

$$\text{s.t. } \mathbf{y}_{\boldsymbol{\tau}(\cdot)}\big(j,\mathbf{y}_k\big) \in \mathbb{Y} \ \forall\, j \in \mathbb{N}_{1,h_p} \tag{16b}$$

with the stage cost ℓ defined in (14). Note that $\mathbb{N}_{1,h_p}$ is considered in (16b) while the summation in (16a) is taken from $j=0$ to h_p-1 since (9) is used in order to predict future states up to $\mathbf{y}_{k+h_p} = \mathbf{y}_{\boldsymbol{\tau}(\cdot)}(h_p,\mathbf{y}_k) = \boldsymbol{\phi}_{\mathbf{y}}\big(\mathbf{y}_{k+h_p-1}, \boldsymbol{\tau}_{k+h_p-1}\big)$ and (16b) ensures that all these predicted future states are feasible.

According to the definition of the proposed stage cost in (14), it is worth highlighting that (15) is an optimization problem nested within the main problem (16). More precisely, the proposed OCP can be classified as a bilevel optimization problem (see [61], [62]), in which the lower level minimization (15) is embedded within the upper level (16). In practice, the solution of the upper level problem (16) cannot be decoupled from the solution of the lower level (15) and each iteration on the numerical solution of (16) should consider updated values of the WE-optimal cable tensions computed according to (15). For further details on the numerical solution of (16), refer to Appendix D.

Note also that, as a consequence of (12) and (15),

$$\|\boldsymbol{\tau}_{wo}(\mathbf{x}_d(k),\boldsymbol{\tau}_{nd}(k)) - \boldsymbol{\tau}_{nd}(k)\|_{\mathbf{K}_{\boldsymbol{\tau}}} + \|\mathbf{y}_d(k)-\mathbf{y}_d(k)\|_{\mathbf{K_y}} = \ell\big(k,\mathbf{y}_d(k),\boldsymbol{\tau}_{nd}(k)\big) = 0 \ \forall\ k \in \mathbb{N} \tag{17}$$

and conditions (13) are satisfied with the stage cost (14). Thereby, the minimal 2-norm tension distribution is performed when solving the OCP (16) , i.e., the cable tension distribution is implicitly performed in real time within the OCP.

In order to exemplify the advantage of this approach, consider $k \in \mathbb{N}$, $\mathbf{y}_k \in \mathbb{Y}$ and a sequence of cable tensions $\hat{\boldsymbol{\tau}}(\cdot) \in \mathbb{U}_k^{h_p}$ that generates an optimal trajectory $\mathbf{y}^*_{\hat{\boldsymbol{\tau}}(\cdot)}(\cdot,\mathbf{y_k}) = \{\mathbf{y}^*_{k+1},\dots,\mathbf{y}^*_{k+h_p}\}$ in the sense that the tracking error

$$\sum_{j=1}^{h_p} \|\mathbf{y}^*_{k+j} - \mathbf{y}_d(k+j)\|_{\mathbf{K_y}} \tag{18}$$

is minimal. A sequence of WE-optimal cable tensions $\boldsymbol{\tau}^*(\cdot)$ defined such that

$$\boldsymbol{\tau}^*_{k+j} = \boldsymbol{\tau}_{wo}(\mathbf{x}_{\mathbf{y}^*_{k+j}}, \hat{\boldsymbol{\tau}}_{k+j}), \forall\, j \in \mathbb{N}_{0,h_p-1} \tag{19}$$

presents minimal 2-norm and generates the very same optimal trajectory $\mathbf{y}^*_{\hat{\boldsymbol{\tau}}(\cdot)}(\cdot,\mathbf{y}_k)$. In accordance with Definition 1, if $\mathbf{y}_k = \mathbf{y}_d(k)$ and $\mathbf{y}_d(\cdot)$ is feasible, $\boldsymbol{\tau}^*_{k+j} = \boldsymbol{\tau}_{nd}(k+j)$ for all $j \in \mathbb{N}_{0,h_p-1}$, $J(k,\mathbf{y}_k,\boldsymbol{\tau}^*(\cdot)) = 0$ and the resulting tracking error is null. The use of the WEO in the stage cost (14) is thus consistent with the minimization of the tracking errors in the sense that WE-optimal cable tensions are able to generate the desired trajectory with null tracking errors. Furthermore, in case of disturbances, modeling uncertainties and unfeasible $\mathbf{y}_d(\cdot)$, the proposed OCP formulation is still able to find an optimal trajectory $\mathbf{y}^*_{\boldsymbol{\tau}^*(\cdot)}(\cdot,\mathbf{y}_k)$ with minimal tracking error and WE-optimal cable tensions $\boldsymbol{\tau}^*(\cdot)$.

IV. Stability Analysis

This section analyzes the stability of the closed-loop system

$$\mathbf{y}_{k+1} = \boldsymbol{\phi}_{\mathbf{y}}\big(\mathbf{y}_k, \boldsymbol{\tau}_{fb}(k,\mathbf{y}_k)\big) \tag{20}$$

obtained with the discrete-time system (8) and the NMPC control policy $\boldsymbol{\tau}_{fb}$ introduced in Algorithm 1-(b) and (16).

To this end, some comparison functions are used. In accordance with commonly used notations [43], [51], the following classes of functions are considered

$$\begin{aligned}
\mathscr{K} &:= \{\alpha : \mathbb{R}^+_0 \to \mathbb{R}^+_0 \mid \alpha \text{ continuous,} \\
&\qquad \text{strictly increasing and } \alpha(0) = 0\}; \\
\mathscr{L} &:= \{\delta : \mathbb{R}^+_0 \to \mathbb{R}^+_0 \mid \delta \text{ continuous,} \\
&\qquad \text{strictly decreasing and } \lim_{t\to\infty} \delta(t) = 0\}; \\
\mathscr{K}\mathscr{L} &:= \{\beta : \mathbb{R}^+_0 \times \mathbb{R}^+_0 \to \mathbb{R}^+_0 \mid \\
&\qquad \beta(r,\cdot) \in \mathscr{L} \text{ and } \beta(\cdot,t) \in \mathscr{K}\} \\
\mathscr{K}_\infty &:= \{\alpha \in \mathscr{K} \mid \alpha \text{ unbounded}\},
\end{aligned}$$

where $\mathbb{R}^+_0 = \{r \in \mathbb{R} \,|\, r \geqslant 0\}$.

Furthermore, for a given sequence $\mathbf{s}^0(\cdot) \in \mathbb{S}^{n_s}$ and instant $k \in \mathbb{N}_0$, special attention will be devoted to a truncated sequence $\mathbf{s}^k(\cdot) = \{\mathbf{s}^0(k),\ \mathbf{s}^0(k+1),\dots\}$. Accordingly, for given

$n_s \in \mathbb{N}$ and $n_i \in \mathbb{N}_0$, the following set of sequences of vectors is introduced:

$$\mathbb{S}_{n_i}^{n_s} = \{\mathbf{s}(\cdot) : \mathbb{N}_{n_i,\infty} \to \mathbb{R}^{n_s}\}. \tag{21}$$

The stability analysis presented in this section deduces sufficient conditions under which the closed-loop system (20) is *uniformly asymptotically stable* according to the following definition.

Definition 2. *Consider the NMPC Algorithm 1 with prediction horizon $h_p \in \mathbb{N}$ and a feasible sequence of desired states $\mathbf{y}_d(\cdot) \in \mathbb{S}^{2n}$. The resulting closed-loop system*

$$\mathbf{y}_{j+1} = \boldsymbol{\phi}_{\mathbf{y}}\left(\mathbf{y}_j, \boldsymbol{\tau}_{fb}(j, \mathbf{y}_j)\right), \ \forall\, j \in \mathbb{N} \tag{22}$$

is called uniformly asymptotically stable to $\mathbf{y}_d(\cdot)$ on $\mathbb{Y}$ if, for each $\mathbf{y}_k \in \mathbb{Y}$ and $k \in \mathbb{N}$, there exists a function $\beta \in \mathscr{KL}$ such that $\mathbf{y}^{fb}(\cdot) \in \mathbb{S}_k^{2n}$ defined according to

$$\begin{aligned} \mathbf{y}_k^{fb} &= \mathbf{y}_k \\ \mathbf{y}_{i+1}^{fb} &= \boldsymbol{\phi}_{\mathbf{y}}\left(\mathbf{y}_i^{fb}, \boldsymbol{\tau}_{fb}(i, \mathbf{y}_i^{fb})\right), \ \forall\ i \in \mathbb{N}_{k,\infty} \end{aligned} \tag{23}$$

satisfies the following relation

$$\|\mathbf{y}_{k+j}^{fb} - \mathbf{y}_d(k+j)\| \leqslant \beta(\|\mathbf{y}_k - \mathbf{y}_d(k)\|, j), \ \forall\ j \in \mathbb{N}. \tag{24}$$

In words, (23) constructs the sequence of states $\mathbf{y}^{fb}(\cdot)$ generated by the closed-loop (22) "departing" from $\mathbf{y}_k$ at sampling time k. The closed-loop (22) takes as feedback control policy $\boldsymbol{\tau}_{fb}$ defined in Algorithm 1. The definition of uniform asymptotic stability presented in Definition 2 is based on an upper bound of the error $\|\mathbf{y}_{k+j}^{fb} - \mathbf{y}_d(k+j)\|$. Note that Definition 2 implicitly assumes $\boldsymbol{\tau}_k = \boldsymbol{\tau}_d(k), \forall k \in \mathbb{N}$, *i.e.* the cable tension control loop (d) in Figure 3 is able to keep a null error.

The upper bound used to limit the tracking error is established in terms of the function $\beta \in \mathscr{KL}$. An illustrative example of a function belonging to this class is presented in Figure 4. In accordance with (IV), for a positive real constant r_0, the illustrative function $\beta_{ex}(r_0, t) = r_0^3/t$ tends to zero for $t \to \infty$ and is strictly decreasing. Since the second argument of β in (24) represents the time, the tracking error asymptotically converges to zero. In contrast, β is strictly increasing with respect to the first argument. Therefore, for increased initial errors $\|\mathbf{y}_k - \mathbf{y}_d(k)\|$, the function of time $\beta(\|\mathbf{y}_k - \mathbf{y}_d(k)\|, \cdot) \in \mathscr{L}$ is increased as well.

Definition 2 is used in [43, Definition 2.16] for the analysis of NMPC schemes and is closely related to [51, Definition 4.2], which is more often used in general nonlinear control. As a matter of fact, the analysis presented in this section is based on [43] and the notations used are similar to those proposed in this reference.

Since the OCP (16) does not use stabilizing terminal conditions, tools designed to analyze NMPC schemes without terminal conditions should be used in the stability analysis of the closed-loop (20). The *minimal time-varying stage cost* denoted by $\ell^* : \mathbb{N} \times \mathbb{Y} \to \mathbb{R}$ is fundamental in this context. This function is defined as

$$\ell^*(k, \mathbf{y}) = \min_{\boldsymbol{\tau} \in \mathbb{U}} \ell(k, \mathbf{y}, \boldsymbol{\tau}). \tag{25}$$

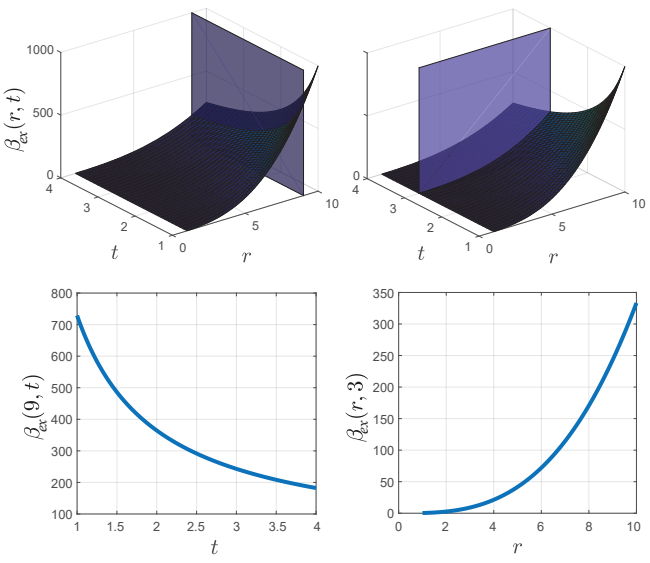

Fig. 4. An illustrative example of a function $\beta_{ex} \in \mathscr{KL}$ given by $\beta_{ex}(r,t) = r^3/t$.

Summarizing some of the results presented in [43, Chapter 6], the following theorem addressing the stability of NMPC schemes without terminal conditions can be stated.

Theorem 1. *Consider the NMPC Algorithm 1 with prediction horizon $h_p \in \mathbb{N}$ and minimal time-varying stage cost satisfying*

$$\begin{aligned} \alpha_1(\|\mathbf{y} - \mathbf{y}_d(k)\|) \leqslant \ell^*(k, \mathbf{y}) \leqslant \alpha_2(\|\mathbf{y} - \mathbf{y}_d(k)\|) \\ \forall\ k \in \mathbb{N} \text{ and } \mathbf{y} \in \mathbb{Y}, \end{aligned} \tag{26}$$

for suitable $\alpha_1, \alpha_2 \in \mathscr{K}_\infty$. Suppose that, for all $\mathbf{y}_k \in \mathbb{Y}$, there exist a feasible $\boldsymbol{\tau}^e(\cdot) \in \mathbb{U}_k^m$, real $C < \infty$ and $\sigma \in (0,1)$ satisfying

$$\ell\left(k+j, \mathbf{y}_{\boldsymbol{\tau}^e(\cdot)}(j, \mathbf{y}_k), \boldsymbol{\tau}_{k+j}^e\right) \leqslant C\,\sigma^j\,\ell^*(k, \mathbf{y}_k), \tag{27}$$

for all $k, j \in \mathbb{N}$. Then, the nominal closed-loop (20) is uniformly asymptotically stable on $\mathbb{Y}$ provided that h_p is sufficiently large.

A draft of the proof of Theorem 1 is presented in Appendix B. This theorem describes sufficient conditions to obtain a stable closed-loop system with the proposed NMPC for h_p sufficiently large.

Conditions (26) will be quite straightforwardly deduced at the end of this section based on (13). Nevertheless, inequality (27) represents an important restriction to the properties of the stage cost. This inequality imposes, for each discrete instant $k \in \mathbb{N}$ and state $\mathbf{y}_k \in \mathbb{Y}$, the existence of a feasible sequence $\boldsymbol{\tau}^e(\cdot)$ that leads to a stage cost $\ell\left(k+j, \mathbf{y}_{\boldsymbol{\tau}^e(\cdot)}(j, \mathbf{y}_k), \boldsymbol{\tau}_j^e\right)$ converging exponentially to zero in time. The exponential convergence is a result of the term $C\,\sigma^j$ with $\sigma \in (0,1)$. Note that the upper bound function $C\,\sigma^j\,\ell^*(k, \mathbf{y}_k)$ is proportional to the initial minimal stage cost $\ell^*(k, \mathbf{y}_k)$.

It is important to highlight that Theorem 1 is based on the existence of *any* feasible sequence $\boldsymbol{\tau}^e(\cdot)$ that satisfies (27). The control policy $\boldsymbol{\tau}_{fb}$ is not considered explicitly in this theorem. In contrast to many control architectures, constrained MPC schemes generally do not have an analytical expression

of the control policy. For this reason, the closed-loop system stability cannot be studied explicitly, but, instead, by means of suitable properties of the stage cost. In this section, these suitable property are given by (26)-(27).

Since one of the terms in the stage cost (14) is the error $\|\mathbf{y}-\mathbf{y}_d\|^2_{\mathbf{K_y}}$, this error needs to be bounded. To this end, the following assumption establishes important properties of the controlled system in order to attain (27).

Assumption 1. *Consider the error* $e_{\mathbf{y}} : \mathbb{N}\times\mathbb{Y}\to\mathbb{R}$ *given by*

$$e_{\mathbf{y}}(k,\mathbf{y}) = \|\mathbf{y}-\mathbf{y}_d(k)\|^2_{\mathbf{K_y}}. \tag{28}$$

For each $\mathbf{y}_k \in \mathbb{Y}$ *and* $k\in\mathbb{N}$*, there exist* $\overline{\boldsymbol{\tau}}(\cdot)\in\mathbb{S}^m_k$*, real* $C_1<\infty$ *and* $\sigma_1\in(0,1)$ *such that*

$$e_{\mathbf{y}}\left(k+j,\mathbf{y}_{\overline{\boldsymbol{\tau}}(\cdot)}(j,\mathbf{y}_k)\right) \leqslant C_1\,\sigma_1^j\, e_{\mathbf{y}}(k,\mathbf{y}_k) \tag{29a}$$

$$\overline{\boldsymbol{\tau}}_{k+j}\in\mathbb{U} \tag{29b}$$

for all $j\in\mathbb{N}_0$.

If Assumption 1 is true, then, for each state $\mathbf{y}_k\in\mathbb{Y}$ and instant $k\in\mathbb{N}$, there exists a feasible sequence of cable tensions $\overline{\boldsymbol{\tau}}(\cdot)$ that generates a trajectory in which the error $\|\mathbf{y}_{\overline{\boldsymbol{\tau}}(\cdot)}(j,\mathbf{y}_k)-\mathbf{y}_d(k+j)\|_{\mathbf{K_y}}$ exponentially converges to zero. Moreover, the upper bound function in (29a) is proportional to the initial errors $e_{\mathbf{y}}(k,\mathbf{y}_k)$. Note that, for given k and $\mathbf{y}_k$, the error $e_{\mathbf{y}}(k,\mathbf{y}_k)$ is constant with respect to the discrete time j. It is easy to show that this assumption is satisfied with a typical control scheme, as detailed in Appendix C. It is interesting to reiterate that the present stability analysis relies on the existence of *any* control sequence satisfying some particular properties. The existence of a control policy satisfying (29a) will be used in order to deduce sufficient conditions to satisfy (27), which plays an important role in the stability analysis of (20).

As important as (29a) imposing the exponential convergence of error $e_{\mathbf{y}}(k,\cdot)$, (29b) requires that the sequence $\overline{\boldsymbol{\tau}}(\cdot)$ is feasible. Considering for instance one of the strategies proposed in [1]–[18], this means that the wrench defined in the feedback motion control policy is feasible for any pose and velocity within the state constraint set $\mathbb{Y}$. Clearly, the definition of the robot workspace and the set $\mathbb{Y}\subset\mathbb{R}^{2n}$ play crucial roles in Assumption 1. The study of the feasibility of a given wrench considering different poses and velocities is addressed in several works (*e.g.* [52]–[56]) and is out of the scope of this paper. Let us also point out that Assumption (29b) is often implicitly taken. Studies such as [4], [6], [10], [63], [64] analyze the corresponding closed-loop systems considering that the feedback loop does not lead to unfeasible cable tensions and, therefore, satisfies (29b).

Since the term $e_{\mathbf{y}}(k,\mathbf{y}) = \|\mathbf{y}-\mathbf{y}_d(k)\|^2_{\mathbf{K_y}}$ in the expression (14) of the stage cost $\ell(k,\mathbf{y},\boldsymbol{\tau})$ is independent of $\boldsymbol{\tau}$, the minimal time-varying stage cost is given by

$$\ell^*(k,\mathbf{y}) = e_{\mathbf{y}}(k,\mathbf{y}) + \min_{\boldsymbol{\tau}\in\mathbb{U}}(\|\boldsymbol{\tau}-\boldsymbol{\tau}_{wo}(\mathbf{x}_{\mathbf{y}},\boldsymbol{\tau})\|^2_{\mathbf{K}_{\boldsymbol{\tau}}}). \tag{30}$$

Lemma 2 will show that the minimum $\min_{\boldsymbol{\tau}\in\mathbb{U}}(\|\boldsymbol{\tau}-\boldsymbol{\tau}_{wo}(\mathbf{x}_{\mathbf{y}},\boldsymbol{\tau})\|_{\mathbf{K}_{\boldsymbol{\tau}}})$ is known and (30) can thus be simplified. Before stating and proving Lemma 2, a preparatory lemma is necessary.

Lemma 1. *Consider* $\boldsymbol{\tau}^a,\boldsymbol{\tau}^b\in\mathbb{U}$ *and* $\mathbf{x}\in\mathbb{X}$*. If* $\mathbf{W}(\mathbf{x})\,\boldsymbol{\tau}^a = \mathbf{W}(\mathbf{x})\,\boldsymbol{\tau}^b$*, then*

$$\boldsymbol{\tau}_{wo}(\mathbf{x},\boldsymbol{\tau}^a) = \boldsymbol{\tau}_{wo}(\mathbf{x},\boldsymbol{\tau}^b). \tag{31}$$

Proof. First, the existence of a $\boldsymbol{\tau}_{wo}(\mathbf{x},\boldsymbol{\tau})$ for all $\mathbf{x}\in\mathbb{R}^n$, $\boldsymbol{\tau}\in\mathbb{U}$ should be proved. The objective function $\|\boldsymbol{\tau}'\|^2$ in (15a) is quadratic and strictly convex. The substitution of $\boldsymbol{\tau}'=\boldsymbol{\tau}\in\mathbb{U}$ in the constraints (15b)-(15c) shows that $\boldsymbol{\tau}$ itself is an element of the set defined by these constraints. Hence, this set is convex and non-empty. Therefore, (15) is a feasible strictly convex inequality constrained Quadratic Programming (QP) problem that possesses a global minimum.

Denoting $\mathbf{f}'\in\mathbb{R}^n$ the wrench such that $\mathbf{f}'=\mathbf{W}(\mathbf{x})\,\boldsymbol{\tau}^a$, Definition (15) indicates that both $\boldsymbol{\tau}_{wo}(\mathbf{x},\boldsymbol{\tau}^a)$ and $\boldsymbol{\tau}_{wo}(\mathbf{x},\boldsymbol{\tau}^b)$ are obtained with

$$\boldsymbol{\tau}_{wo}(\mathbf{x},\boldsymbol{\tau}^a) = \boldsymbol{\tau}_{wo}(\mathbf{x},\boldsymbol{\tau}^b) = \arg\min_{\boldsymbol{\tau}'}\ \|\boldsymbol{\tau}'\|_2^2 \tag{32a}$$

$$\text{s.t. } \mathbf{W}(\mathbf{x})\,\boldsymbol{\tau}' = \mathbf{f}' \tag{32b}$$

$$\boldsymbol{\tau}_{min}\leqslant\boldsymbol{\tau}'\leqslant\boldsymbol{\tau}_{max} \tag{32c}$$

and, therefore, (31) is true. □

Lemma 1 shows that if two vectors of cable tensions generate the same wrench in a given pose, they lead to the same WE-optimal tension distribution. The following corollary is based on this result.

Corollary 1. *For every* $\boldsymbol{\tau}^a,\boldsymbol{\tau}^b\in\mathbb{U}$ *and* $\mathbf{x}\in\mathbb{X}$*, if*

$$\boldsymbol{\tau}^b = \boldsymbol{\tau}_{wo}(\mathbf{x},\boldsymbol{\tau}^a), \tag{33}$$

then

$$\boldsymbol{\tau}^b = \boldsymbol{\tau}_{wo}(\mathbf{x},\boldsymbol{\tau}^b). \tag{34}$$

Proof. Taking $\boldsymbol{\tau}^a$, $\boldsymbol{\tau}^b$ and $\mathbf{x}$ from the corollary statement such that $\boldsymbol{\tau}^b=\boldsymbol{\tau}_{wo}(\mathbf{x},\boldsymbol{\tau}^a)$, constraints (15b)-(15c) in the definition of $\boldsymbol{\tau}_{wo}$ implies that $\mathbf{W}(\mathbf{x})\,\boldsymbol{\tau}^a=\mathbf{W}(\mathbf{x})\,\boldsymbol{\tau}^b$ and $\boldsymbol{\tau}^b\in\mathbb{U}$. Therefore, applying Lemma 1, $\boldsymbol{\tau}_{wo}(\mathbf{x},\boldsymbol{\tau}^a)=\boldsymbol{\tau}_{wo}(\mathbf{x},\boldsymbol{\tau}^b)$, and thanks to (33), this leads to $\boldsymbol{\tau}^b=\boldsymbol{\tau}_{wo}(\mathbf{x},\boldsymbol{\tau}^b)$. □

Lemma 2. *For every* $\mathbf{y}\in\mathbb{Y}$*,* $\boldsymbol{\tau}\in\mathbb{U}$ *and* $k\in\mathbb{N}$*,*

$$\min_{\boldsymbol{\tau}\in\mathbb{U}}(\|\boldsymbol{\tau}-\boldsymbol{\tau}_{wo}(\mathbf{x}_{\mathbf{y}},\boldsymbol{\tau})\|^2_{\mathbf{K}_{\boldsymbol{\tau}}}) = 0, \tag{35}$$

and the minimal time-varying stage cost is given by

$$\ell^*(k,\mathbf{y}) = \|\mathbf{y}-\mathbf{y}_d(k)\|^2_{\mathbf{K_y}} = e_{\mathbf{y}}(k,\mathbf{y}). \tag{36}$$

Proof. For every $\mathbf{y}\in\mathbb{Y}$ and $\boldsymbol{\tau}\in\mathbb{U}$, one may set $\boldsymbol{\tau}_{out}=\boldsymbol{\tau}_{wo}(\mathbf{x}_{\mathbf{y}},\boldsymbol{\tau})$, and thanks to the constraints (15c), $\boldsymbol{\tau}_{out}\in\mathbb{U}$. Moreover, we have $\|\boldsymbol{\tau}_{out}-\boldsymbol{\tau}_{wo}(\mathbf{x}_{\mathbf{y}},\boldsymbol{\tau})\|^2_{\mathbf{K}_{\boldsymbol{\tau}}}=0$. Since the expression $\|\boldsymbol{\tau}-\boldsymbol{\tau}_{wo}(\mathbf{x},\boldsymbol{\tau})\|^2_{\mathbf{K}_{\boldsymbol{\tau}}}=0$ is non-negative, this proves (35). Substituting (35) in (30), equation (36) is obtained. □

As discussed in Section III, $\boldsymbol{\tau}_{wo}(\mathbf{x},\boldsymbol{\tau})$ is the vector of cable tensions with minimal 2-norm that generates the same wrench as $\boldsymbol{\tau}$ in pose $\mathbf{x}$. Loosely speaking, the influence of $\boldsymbol{\tau}_{wo}(\mathbf{x},\boldsymbol{\tau})$ and $\boldsymbol{\tau}$ on the system dynamics should be equivalent. This equivalence is described in a more precise manner in the following assumption.

Assumption 2. *Consider* $\mathbf{y}, \mathbf{y}^+ \in \mathbb{Y}$ *and* $\boldsymbol{\tau}^a, \boldsymbol{\tau}^b \in \mathbb{U}$. *If these vectors satisfy*

$$\mathbf{y}^+ = \boldsymbol{\phi}_{\mathbf{y}}(\mathbf{y}, \boldsymbol{\tau}^a) \text{ and} \tag{37a}$$

$$\mathbf{W}(\mathbf{x}_{\mathbf{y}})\,\boldsymbol{\tau}^b = \mathbf{W}(\mathbf{x}_{\mathbf{y}})\,\boldsymbol{\tau}^a \tag{37b}$$

then, the following relation also holds:

$$\mathbf{y}^+ = \boldsymbol{\phi}_{\mathbf{y}}(\mathbf{y}, \boldsymbol{\tau}^b) = \boldsymbol{\phi}_{\mathbf{y}}(\mathbf{y}, \boldsymbol{\tau}^a). \tag{38}$$

It is easy to demonstrate that Assumption 2 is satisfied with the transition mapping (7). It can be noted that this assumption is implicitly taken if the stability of a digital control system is analyzed considering the robot controller as a continuous-time system, as in [4], [6], [10], [63], [64].

Based on Assumption 2, for a given initial state vector, two sequences of cable tensions that generate identical wrenches at the corresponding poses result in identical trajectories. Therefore, any trajectory performed with an arbitrary sequence of feasible cable tensions can also be generated with an alternative sequence consisting of WE-optimal tensions generating the same wrenches along the trajectory. With the latter cable tension sequence, the stage cost at each instant along the trajectory is equal to the minimal time-varying cost ℓ^*. This assertion is rigorously formulated in Lemma 3.

Lemma 3. *For each* $\mathbf{y}_k \in \mathbb{Y}$, $\mathbf{y}(\cdot) \in \mathbb{S}^{2n}_k$ *and* $\boldsymbol{\tau}(\cdot) \in \mathbb{S}^m_k$ *such that, for all* $j \in \mathbb{N}_0$,

$$\mathbf{y}_{k+j} = \mathbf{y}_{\boldsymbol{\tau}(\cdot)}(j, \mathbf{y}_k) \in \mathbb{Y} \tag{39a}$$

$$\boldsymbol{\tau}_{k+j} \in \mathbb{U}, \tag{39b}$$

if Assumption 2 holds, there exists a $\boldsymbol{\tau}^*(\cdot) \in \mathbb{S}^m_k$ *that satisfies*

$$\mathbf{y}_{\boldsymbol{\tau}(\cdot)}(j, \mathbf{y}_k) = \mathbf{y}_{\boldsymbol{\tau}^*(\cdot)}(j, \mathbf{y}_k) = \mathbf{y}_{k+j}, \tag{40a}$$

$$\boldsymbol{\tau}_{wo}(\mathbf{x}_{\mathbf{y}_{k+j}}, \boldsymbol{\tau}^*_{k+j}) = \boldsymbol{\tau}^*_{k+j} \in \mathbb{U} \tag{40b}$$

$$\ell(k+j, \mathbf{y}_{k+j}, \boldsymbol{\tau}^*_{k+j}) = e_{\mathbf{y}}(k+j, \mathbf{y}_{k+j}) = \ell^*(k+j, \mathbf{y}_{k+j}) \tag{40c}$$

for all $j \in \mathbb{N}_0$.

Proof. For $\mathbf{y}_k$, $\mathbf{y}(\cdot)$ and $\boldsymbol{\tau}(\cdot)$ stated in the lemma, define $\boldsymbol{\tau}^*(\cdot) \in \mathbb{S}^m_k$ and $\mathbf{y}^*(\cdot) \in \mathbb{S}^{2n}_k$ as

$$\begin{aligned} \boldsymbol{\tau}^*_{k+j} &= \boldsymbol{\tau}_{wo}(\mathbf{x}_{\mathbf{y}_{k+j}}, \boldsymbol{\tau}_{k+j}), \\ \mathbf{y}^*_{k+j} &= \mathbf{y}_{\boldsymbol{\tau}^*(\cdot)}(j, \mathbf{y}_k) \end{aligned} \tag{41}$$

for all $j \in \mathbb{N}_0$. Due to the constraint (15b),

$$\mathbf{W}(\mathbf{x}_{\mathbf{y}_k})\,\boldsymbol{\tau}_k = \mathbf{W}(\mathbf{x}_{\mathbf{y}_k})\,\boldsymbol{\tau}^*_k \tag{42}$$

and, according to (38) and (9),

$$\mathbf{y}^*_{k+1} = \mathbf{y}_{\boldsymbol{\tau}^*(\cdot)}(1, \mathbf{y}_k) = \boldsymbol{\phi}_{\mathbf{y}}(\mathbf{y}_k, \boldsymbol{\tau}^*_k) = \mathbf{y}_{k+1}. \tag{43}$$

Moreover, (41)-(42) and Lemma 1 imply that

$$\boldsymbol{\tau}_{wo}(\mathbf{x}_{\mathbf{y}_k}, \boldsymbol{\tau}^*_k) = \boldsymbol{\tau}_{wo}(\mathbf{x}_{\mathbf{y}_k}, \boldsymbol{\tau}_k) = \boldsymbol{\tau}^*_k. \tag{44}$$

By induction, one can obtain

$$\begin{aligned} \mathbf{y}^*_{k+2} &= \boldsymbol{\phi}_{\mathbf{y}}(\mathbf{y}_{k+1}, \boldsymbol{\tau}^*_{k+1}) = \mathbf{y}_{k+2} \\ \mathbf{y}^*_{k+3} &= \boldsymbol{\phi}_{\mathbf{y}}(\mathbf{y}_{k+2}, \boldsymbol{\tau}^*_{k+2}) = \mathbf{y}_{k+3} \\ &\vdots \end{aligned} \tag{45}$$

and

$$\begin{aligned} \boldsymbol{\tau}_{wo}(\mathbf{x}_{\mathbf{y}_{k+1}}, \boldsymbol{\tau}^*_{k+1}) &= \boldsymbol{\tau}_{wo}(\mathbf{x}_{\mathbf{y}_{k+1}}, \boldsymbol{\tau}_{k+1}) = \boldsymbol{\tau}^*_{k+1} \\ \boldsymbol{\tau}_{wo}(\mathbf{x}_{\mathbf{y}_{k+2}}, \boldsymbol{\tau}^*_{k+2}) &= \boldsymbol{\tau}_{wo}(\mathbf{x}_{\mathbf{y}_{k+2}}, \boldsymbol{\tau}_{k+2}) = \boldsymbol{\tau}^*_{k+2} \\ &\vdots \end{aligned} \tag{46}$$

which are equivalent to (40a) and (40b).

Equation (40b) and Lemma 2 imply that

$$\begin{aligned} &\ell(k+j, \mathbf{y}_{k+j}, \boldsymbol{\tau}^*_{k+j}) = \\ &\quad e_{\mathbf{y}}(k+j, \mathbf{y}_{k+j}) + \|\boldsymbol{\tau}^*_{k+j} - \boldsymbol{\tau}_{wo}(\mathbf{x}_{\mathbf{y}_{k+j}}, \boldsymbol{\tau}^*_{k+j})\|_{\mathbf{K}_{\boldsymbol{\tau}}} = \\ &\quad e_{\mathbf{y}}(k+j, \mathbf{y}_{k+j}) = \ell^*(k+j, \mathbf{y}_{k+j}), \end{aligned} \tag{47}$$

as in (40c). □

Finally, the main results on the stability of the NMPC scheme proposed in Section III are summarized in the following theorem.

Theorem 2. *Consider the NMPC Algorithm 1 with prediction horizon* $h_p \in \mathbb{N}$ *and feasible desired trajectory* $\mathbf{y}_d(\cdot) \in \mathbb{S}^{2n}$. *Consider also that Assumptions 1 and 2 hold. Then, the nominal closed-loop system* (20) *is uniformly asymptotically stable on* $\mathbb{Y}$ *provided that* h_p *is sufficiently large.*

Proof. The proof consists in analyzing the conditions presented in Theorem 1. First, it is necessary to prove that there exist $\alpha_1, \alpha_2 \in \mathscr{K}_\infty$ such that

$$\begin{aligned} \alpha_1(\|\mathbf{y} - \mathbf{y}_d(k)\|) \leqslant \ell^*(k, \mathbf{y}) \leqslant \alpha_2(\|\mathbf{y} - \mathbf{y}_d(k)\|) \\ \forall\ k \in \mathbb{N} \text{ and } \mathbf{y} \in \mathbb{Y}. \end{aligned} \tag{48}$$

According to Lemma 2, $\ell^*(k, \mathbf{y}) = \|\mathbf{y} - \mathbf{y}_d(k)\|^2_{\mathbf{K}_{\mathbf{y}}}$ such that the following inequalities hold for all $k \in \mathbb{N}$:

$$\begin{aligned} K^{min}_{\mathbf{y}} \|\mathbf{y} - \mathbf{y}_d(k)\|^2 &\leqslant \ell^*(k, \mathbf{y}) \\ &= \|\mathbf{y} - \mathbf{y}_d(k)\|^2_{\mathbf{K}_{\mathbf{y}}} \\ &\leqslant K^{max}_{\mathbf{y}} \|\mathbf{y} - \mathbf{y}_d(k)\|^2. \end{aligned} \tag{49}$$

where $K^{min}_{\mathbf{y}}$ and $K^{max}_{\mathbf{y}}$ are the minimum and maximum singular value of $\mathbf{K}_{\mathbf{y}}$, respectively.

Defining $\alpha_1, \alpha_2 \in \mathscr{K}_\infty$ by $\alpha_1(r) = K^{min}_{\mathbf{y}} r^2$ and $\alpha_2(r) = K^{max}_{\mathbf{y}} r^2$, (49) can be written as

$$\alpha_1(\|\mathbf{y} - \mathbf{y}_d(k)\|) \leqslant \ell^*(k, \mathbf{y}) \leqslant \alpha_2(\|\mathbf{y} - \mathbf{y}_d(k)\|)\ \forall\ k \in \mathbb{N}, \tag{50}$$

which proves (26).

In addition, (27) should be proved. If Assumption 1 holds, then for each $\mathbf{y}_k \in \mathbb{Y}$ and $k \in \mathbb{N}$, there exist $\overline{\boldsymbol{\tau}}(\cdot) \in \mathbb{S}^m_k$, real $C_1 < \infty$ and $\sigma_1 \in (0, 1)$ such that

$$e_{\mathbf{y}}\left(k+j, \mathbf{y}_{\overline{\boldsymbol{\tau}}(\cdot)}(j, \mathbf{y}_k)\right) \leqslant C_1\, \sigma_1^j\, e_{\mathbf{y}}(k, \mathbf{y}_k) \tag{51a}$$

$$\overline{\boldsymbol{\tau}}_{k+j} \in \mathbb{U} \tag{51b}$$

for all $j \in \mathbb{N}_0$. Applying Lemma 3 with $\boldsymbol{\tau}(\cdot) = \overline{\boldsymbol{\tau}}(\cdot)$, the obtained sequence $\boldsymbol{\tau}^*(\cdot)$ leads to the same trajectory (as implied by (40a)) and, therefore, (51a) remains valid. In addition, (40c) implies that

$$\ell\big(k+j, \mathbf{y}_{\boldsymbol{\tau}^*(\cdot)}(j, \mathbf{y}_k), \boldsymbol{\tau}^*_{k+j}\big) = e_{\mathbf{y}}(k+j, \mathbf{y}_{\boldsymbol{\tau}^*(\cdot)}(j, \mathbf{y}_k)) \tag{52a}$$

$$\leqslant C_1\, \sigma_1^j\, e_{\mathbf{y}}(k, \mathbf{y}_k) \tag{52b}$$

$$= C_1\, \sigma_1^j\, \ell^*(k, \mathbf{y}_k), \tag{52c}$$

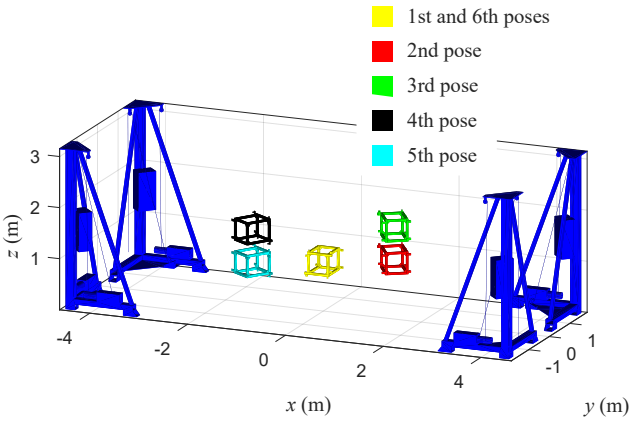

Fig. 5. Visited poses for the pick-and-place trajectories performed in the numerical simulations.

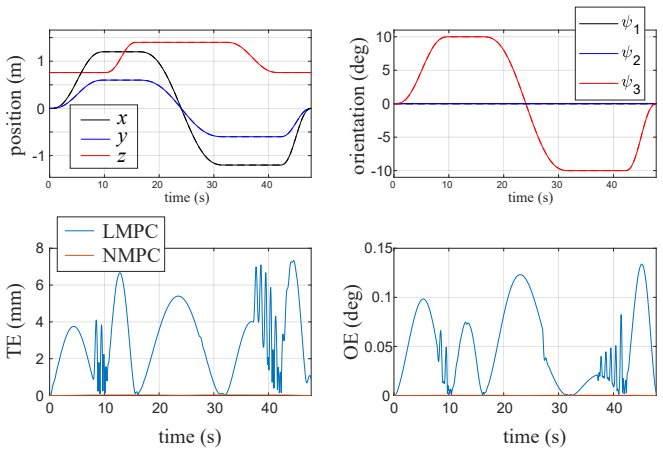

Fig. 6. Numerical results comparing LMPC and NMPC schemes with optimal gains.

where (51a) and (36) were used in order to obtain (52b) and (52c), respectively. Inequality (52) proves (27), finalizing the stability analysis. □

V. Numerical Simulations

The performance of the proposed NMPC scheme is compared through numerical simulations to the LMPC introduced in [28]. Typical pick-and-place trajectories are used and the dimensions of CDPR prototype HRPCable are considered (see Figures 1 and 2). The technical characteristics of this CDPR prototype are discussed more in detail in the next section.

Instead of the stage cost $\ell(k,\mathbf{y},\boldsymbol{\tau})$ as in (14), the LMPC of [28] is based on the cost function $\ell_{LMPC}:\mathbb{N}_0\times\mathbb{Y}\times\mathbb{U}\times\mathbb{U}\to\mathbb{R}$ defined as

$$\ell_{LMPC}(k,\mathbf{y},\boldsymbol{\tau}_k,\boldsymbol{\tau}_{k-1}) = \|\mathbf{y}-\mathbf{y}_d(k)\|^2_{\mathbf{K}_1} + c_2\|\boldsymbol{\tau}_k\|^2 + \\ + c_3\|\boldsymbol{\tau}_k-\boldsymbol{\tau}_{k-1}\|^2, \tag{53}$$

where c_2, c_3 are positive real constants, $\mathbf{K}_1=\text{diag}(\mathbf{k}_1)$ with $\mathbf{k}_1\in\mathbb{R}^{2n}_+$ and $\|\boldsymbol{\tau}_k-\boldsymbol{\tau}_{k-1}\|$ represents the 2-norm of the variation of the cable tensions between sampling times $k-1$ and k. More details on LMPC schemes for the position tracking of CDPRs are presented in [28], [65].

Optimal controller gains for both the LMPC from [28] and the NMPC proposed in Section III were obtained through Particle Swarm Optimization (PSO). These optimizations were based on the trajectories depicted in Figures 5 and 6. The platform orientation is defined by three Euler angles ψ_1, ψ_2, ψ_3. More precisely, the rotation matrix used in (63) is given by

$$\mathbf{R}(\boldsymbol{\psi}) = \mathbf{R}_z(\psi_3)\,\mathbf{R}_y(\psi_2)\,\mathbf{R}_x(\psi_1), \tag{54}$$

with $\mathbf{R}_x,\mathbf{R}_y,\mathbf{R}_z:\mathbb{R}\to\mathbb{R}^{3\times3}$ the elementary rotation matrices around x, y and z axes, respectively. The cable tension limits are taken as $\boldsymbol{\tau}_{min}=100$ N and $\boldsymbol{\tau}_{max}=400$ N.

Considering the desired trajectory shown in Figure 5, the simulation of the closed-loop system obtained with the LMPC scheme using a given set of gains $\{\mathbf{k}_1,c_2,c_3\}$ leads to translation errors $\text{TE}(k)$ and orientation errors $\text{OE}(k)$ for any instant k within the time interval corresponding to the trajectory motion. Accordingly, the optimal LMPC gains were obtained by means of the minimization of a weighted sum of the maximum translation and orientation errors, *i.e.*:

$$\{\mathbf{k}_1^*,c_2^*,c_3^*\} = \underset{\{\mathbf{k}_1,c_2,c_2\}}{\arg\min}\left(w_t\max_k \text{TE}(k) + w_o\max_k \text{OE}(k)\right),$$

for positive constant weights w_t and w_o. Optimal NMPC gains $\{\mathbf{k}_\mathbf{y}^*,\mathbf{k}_{\boldsymbol{\tau}}^*\}$ were obtained with an equivalent procedure and using the same weights w_t and w_o. The sampling period of both control schemes was considered as $\Delta t=22$ ms. The NMPC prediction horizon was defined as $h_p=4$ while the LMPC prediction horizon was taken as $h_{p,LMPC}=8$. A NMPC prediction horizon smaller than the LMPC one was chosen in order to compensate for the increased complexity of the optimal control problem addressed within the NMPC strategy. These parameter values are in accordance with the experimental tests presented in Section VI.

Figure 6 compares the errors obtained with the LMPC and NMPC schemes using the corresponding optimal control gains. Relatively small errors are obtained with the LMPC scheme since $\text{TE}(k)<8$ mm and $\text{OE}(k)<0.15$ degrees for all k in the trajectory time interval. However, the NMPC control strategy proposed in this paper performs much better as it is able to maintain errors virtually equal to zero, namely, $\text{TE}(k)<0.03$ mm and $\text{OE}(k)<2\times10^{-4}$ degrees for all k in the trajectory time interval. These results are consistent with the discussion presented in Section III. Namely, while the LMPC minimizes the cable tensions in detriment of the tracking errors, the proposed NMPC scheme is able to compute an optimal cable tension distribution without degrading the tracking errors.

In order to better illustrate the contrast between these two control schemes, the values of the maximum translation and orientation errors were evaluated for different controller gains. More precisely, Figure 7 compares the errors obtained with sets of random controller gain values uniformly distributed within the intervals given by

$$\begin{cases} 0.5\times\mathbf{k}_\mathbf{y}^* \leqslant \mathbf{k}_\mathbf{y} \leqslant 1.5\times\mathbf{k}_\mathbf{y}^* \\ 0.5\times\mathbf{k}_{\boldsymbol{\tau}}^* \leqslant \mathbf{k}_{\boldsymbol{\tau}} \leqslant 1.5\times\mathbf{k}_{\boldsymbol{\tau}}^* \end{cases} \tag{55}$$

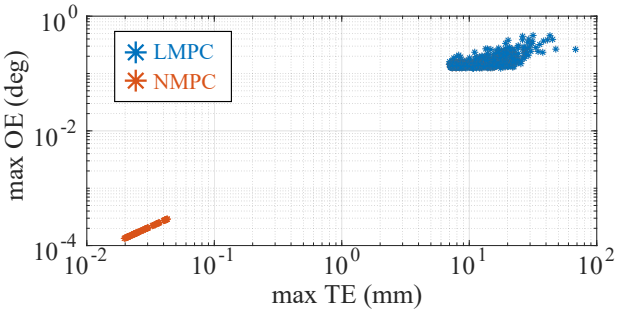

Fig. 7. Monte Carlo simulation comparing LMPC and NMPC schemes for different controller gains.

for the NMPC, and

$$\begin{cases} 0.5 \times \mathbf{k}_1^* \leqslant \mathbf{k}_1 \leqslant 1.5 \times \mathbf{k}_1^* \\ 0.5 \times c_2^* \leqslant c_2 \leqslant 1.5 \times c_2^* \\ 0.5 \times c_3^* \leqslant c_3 \leqslant 1.5 \times c_3^* \end{cases} \tag{56}$$

for the LMPC. The logarithmic plot chart depicted in Figure 7 indicates that the sets of NMPC controller gains $\{\mathbf{k}_\mathbf{y}, \mathbf{k}_{\boldsymbol{\tau}}\}$ within the intervals (55) lead to $\mathrm{TE}(k) < 0.1$ mm and $\mathrm{OE}(k) < 10^{-3}$ degrees. In contrast, as shown in Figure 7, the 1300 different LMPC controller gains sampled in intervals (56) yield $\max_k \mathrm{TE}(k) > 7.0$ mm and $\max_k \mathrm{OE}(k) > 0.12$ degrees.

VI. Experimental Validation

The NMPC scheme proposed in Section III was implemented on the HRPCable prototype (Figure 1) leading to the experimental results detailed in the present section. HRPCable is a 6-DoF CDPR fully-constrained by eight cables. Its dimensions are shown in Figures 2 and 9. The robot is essentially built with Beckhoff components typically used in industry. Each winch is equipped with a servo drive AX5112, a motor AM8061 and gear train AG2210. An industrial PC C6920 equipped with an Intel 2.4GHz i7 core processor communicates with the servo drives through EtherCAT protocol. Cable tensions are measured with load pins Sensy 5300 1T SL positioned in the axes of the routing pulleys. The platform is a cube with length equal to 1 m and total mass $m_p = 23$ kg.

Apart from the mechanical components, the presented experimental results were obtained using the industrial software TwinCAT [66]. This software is not compatible with libraries commonly used for matrix manipulation. For this reason, the proposed NMPC scheme was developed from scratch. The environment in which the controller was implemented proves the applicability of the proposed solutions in the industry. Appendix D presents details on the numerical implementation of the control algorithm introduced in Section III. The results presented in this section also use the kinematic model and cable tension control (blocks (b), (c) and (d) in Figure 3) introduced in [60] and [57], respectively.

Similarly to the previous section, the performance of the proposed NMPC scheme is compared to the LMPC introduced in [28] using typical pick-and-place trajectories. These control schemes are also compared with respect to their robustness against payload uncertainties.

In addition, an unfeasible desired trajectory is used in order to show that the proposed NMPC scheme can operate on the boundaries of the robot WFW without failure. While the proposed NMPC scheme is able to track a trajectory as close as possible to an unfeasible desired trajectory, a state-of-the-art control scheme leads to a sudden interruption of the robot operation. The results obtained with the proposed NMPC scheme were summarized in a video[1] that has been attached to the present paper.

Taking the optimal gains obtained in the previous section as initial estimation, the NMPC control parameters used in the experimental tests presented in this section were tuned by trial and error. Defining $\mathbf{k}_\mathbf{x}, \mathbf{k}_{\dot{\mathbf{x}}} \in \mathbb{R}^n_+$ as subvectors of $\mathbf{k}_\mathbf{y}$ such that $\mathbf{k}_\mathbf{y} = \begin{bmatrix} \mathbf{k}_\mathbf{x}^T & \mathbf{k}_{\dot{\mathbf{x}}}^T \end{bmatrix}^T$, the used controller parameters can be summarized as follows:

$$\mathbf{K}_\mathbf{y} = \mathrm{diag}(\begin{bmatrix} \mathbf{k}_\mathbf{x}^T & \mathbf{k}_{\dot{\mathbf{x}}}^T \end{bmatrix}^T) \tag{57a}$$

$$\mathbf{k}_\mathbf{x} = \begin{bmatrix} 56 & 68 & 48 & 52 & 52 & 36 \end{bmatrix}^T \tag{57b}$$

$$\mathbf{k}_{\dot{\mathbf{x}}} = \begin{bmatrix} 11 & 13 & 9 & 10 & 10 & 7 \end{bmatrix}^T \tag{57c}$$

$$\mathbf{K}_{\boldsymbol{\tau}} = 6 \times 10^{-7}\,\mathbf{I} \text{ and } h_p = 4. \tag{57d}$$

As in the previous section, the cycle time of the cable tension control (block (d) in Figure 3) is 2 ms while the one used for the NMPC controller is $\Delta t = 22$ ms. The sampling period of the cable tension control is mainly limited by the response time of the velocity control loop (which is managed at the servo drives) while the cycle time $\Delta t = 22$ ms of the NMPC control loop is limited by the time required to solve the OCP (16) in real time.

A. Pick-and-place trajectories

The desired trajectories representing typical pick-and-place tasks are defined using fifth-degree polynomials based on the CDPR mobile platform poses depicted in Figure 9. Two scenarios of maximum cable tension are considered: (i) $\boldsymbol{\tau}_{max} = 400$ N and (ii) $\boldsymbol{\tau}_{max} = 250$ N. These scenarios are addressed respectively in Sections VI-A1 and VI-A2 and both cases consider $\boldsymbol{\tau}_{min} = 100$ N.

1) Nominal cable tension limits: Figure 8 shows the experimental results obtained using the proposed NMPC scheme taking cable tension limits $\boldsymbol{\tau}_{min} = 100$ N and $\boldsymbol{\tau}_{max} = 400$ N. Tracking errors consist of the Translation Errors (TE) and Orientation Errors (OE). Figure 8 also depicts the cable tensions measured using the aforementioned load pins.

The same trajectory was performed with the LMPC proposed in [28]. Figure 10 compares the corresponding results. In accordance with the goals defined in the present paper, the comparative results presented in Figure 10 indicate that the proposed NMPC scheme leads to significantly better tracking errors than the LMPC approach. Indeed, Table I shows that substantial improvements were obtained considering both the RMS of the tracking errors and the maximum errors. These errors are based on the platform pose computed by the forward kinematics (block (b) in Figure 3).

[1]HD video available in `https://youtu.be/NIb_XYSVv84`

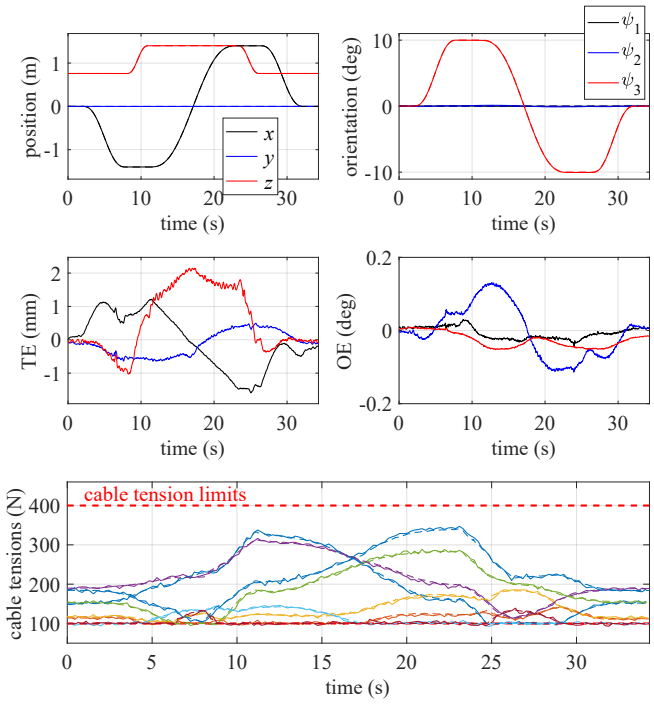

Fig. 8. Experimental results for $\boldsymbol{\tau}_{max} = 400$ N. In the charts presenting the cable tensions, the dashed and solid lines represent the desired and measured tensions, respectively.

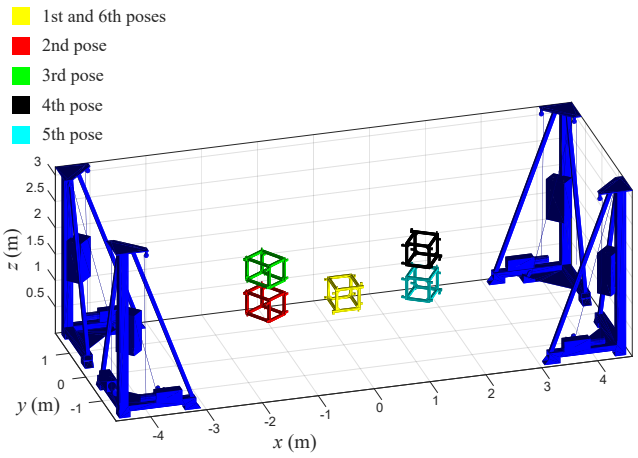

Fig. 9. Visited poses for the pick-and-place trajectories performed in the experimental tests.

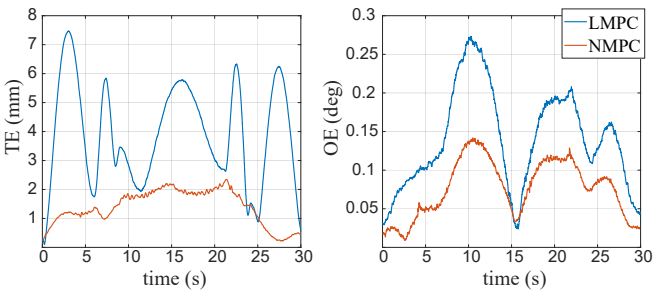

Fig. 10. Tracking errors of LMPC and NMPC schemes for the pick-and-place trajectory with $\boldsymbol{\tau}_{max} = 400$ N.

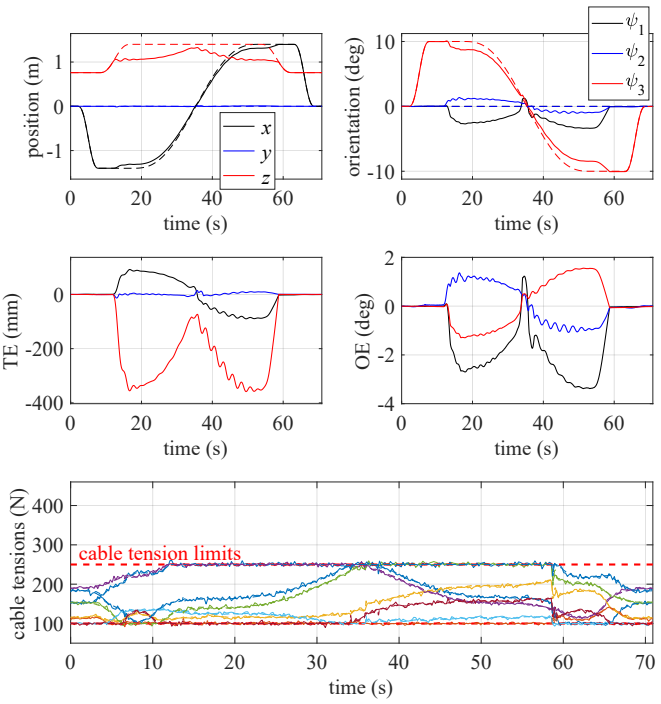

Fig. 11. Experiments with $\boldsymbol{\tau}_{max} = 250$ N. In the charts presenting the platform position and orientation, the dashed and solid lines represent the desired and actual trajectories, respectively.

TABLE I
SUMMARY OF COMPARATIVE ERRORS BETWEEN LMPC AND NMPC: ROOT MEAN SQUARE (RMS), STANDARD DEVIATION (SD) AND MAXIMUM ERRORS.

	RMS (SD)		Maximum error	
	TE	OE	TE	OE
LMPC	4.28 (2.17) mm	0.15 (0.07) °	7.47 mm	0.27°
NMPC	1.52 (0.76) mm	0.08 (0.04) °	2.34 mm	0.14°
Improvement	64.5 (64.8) %	44.6 (42.1) %	68.6%	48.1%

2) Reduced maximum cable tension: The authors' previous study [28] highlighted that the main contribution of the corresponding LMPC scheme lies in its capability to handle cable tension limits explicitly. Thanks to this characteristic, this LMPC is not prone to the feasibility issues discussed in Section I. In order to verify this property, an unfeasible desired trajectory was used in [28]. The same behavior should be validated for the NMPC scheme proposed in the present paper.

Therefore, a second scenario is considered taking a maximum cable tension reduced to $\boldsymbol{\tau}_{max} = 250$ N. The same path depicted in Figure 9 is also used in this case with reduced maximum tension. The obtained results are shown in Figure 11. Although the desired trajectory escapes from the WFW defined by this reduced maximum tension, the proposed control scheme is able to track a trajectory as close as possible to the desired one without violating the cable tension limits.

Therefore, as demonstrated in this experiment, the main advantage of the proposed NMPC scheme with respect to state-of-the-art strategies such as [1]–[18] lies in its capability to operate on the robot WFW boundaries without failure. The

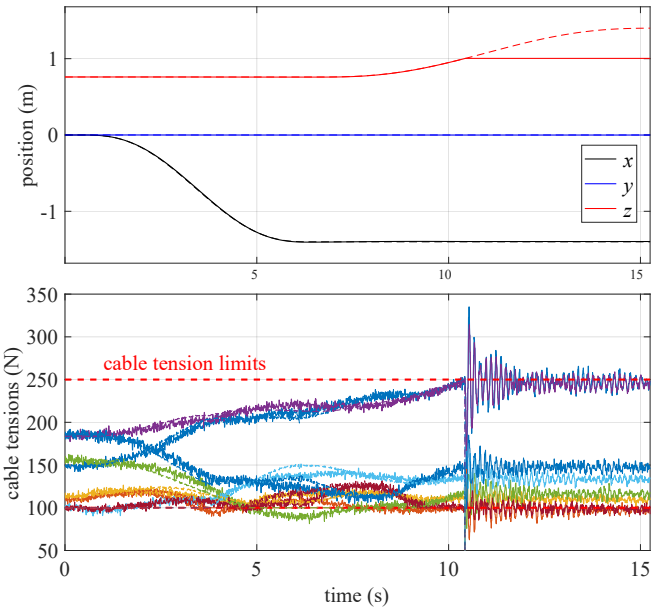

Fig. 12. Experimental results obtained with the control scheme proposed in [5] with the reduced maximum cable tension $\boldsymbol{\tau}_{max} = 250$ N. The robot operation is terminated at $t \approx 10.5$ s, when the cable tensions become unfeasible.

control strategies proposed in [1]–[18] combined with some of the tension distribution algorithms in [21]–[26] would fail to fulfill this objective. As an example, Figure 12 presents the experimental results obtained using the control scheme proposed in [5]. As soon as the desired trajectory reaches unfeasible poses, the robot operation is terminated because the controller requires the tension distribution module to compute an unfeasible wrench.

It is worth noting that the results presented in this section consider the state constraint set $\mathbb{Y}$ equal to $\mathbb{R}^{2n}$. Hence, only the cable tension constraint set $\mathbb{U}$, *i.e.*, the WFW, limits the operation range of the NMPC scheme. This exempts the control designer from the potentially arduous task of defining the set $\mathbb{Y}$. Moreover, the solution of (16) is also facilitated by the reduced number of constraints.

In addition, one may note that the velocities of the trajectory depicted in Figure 11 are lower than those of the original trajectory shown in Figure 8. Lower velocities were used in order to reduce platform oscillations when the desired trajectory escapes the WFW. Alternatively, results of [28] show that the addition to the stage cost of a term $\|\boldsymbol{\tau}_k - \boldsymbol{\tau}_{k-1}\|$ penalizing cable tension variations is an efficient method to reduce these oscillations. Nevertheless, nontrivial modifications of the stability analysis of Section IV would be necessary in this case. Accordingly, for the sake of consistency, the results presented in this section do not apply a penalization of $\|\boldsymbol{\tau}_k - \boldsymbol{\tau}_{k-1}\|$.

B. Robustness against payload uncertainties

CDPRs are often used in order to handle relatively heavy payloads. Typically, the weight of such payloads are not precisely known. Therefore, the tracking accuracy under the incidence of payload uncertainties is a crucial aspect to be considered in the analysis of CDPR position tracking control.

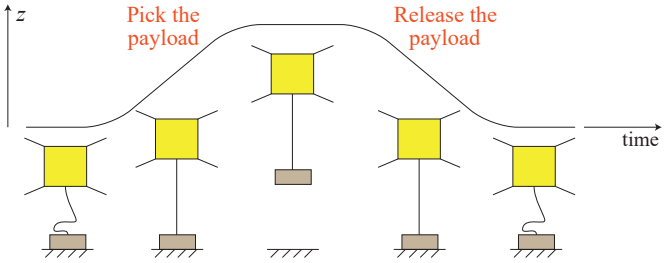

Fig. 13. Illustration of the robustness test.

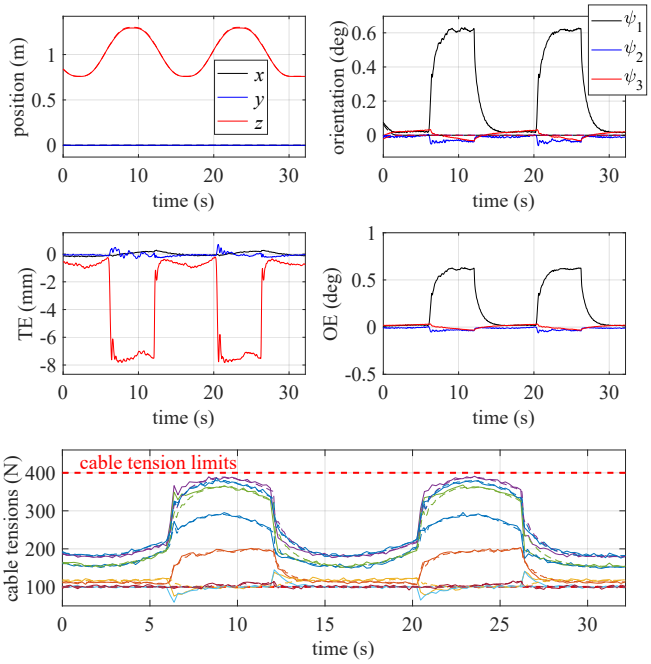

Fig. 14. Experimental results obtained with the NMPC scheme in the experiment evaluating the robustness against payload uncertainties.

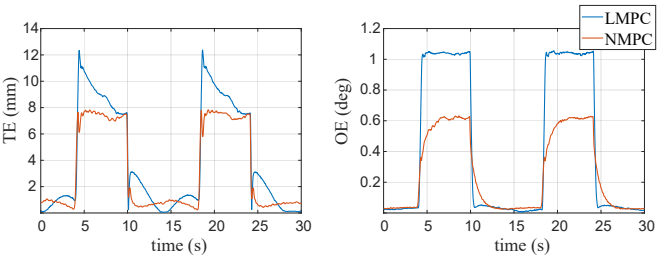

Fig. 15. Tracking errors of the LMPC and NMPC schemes in the experiment testing the robustness against payload uncertainties.

Accordingly, in addition to the presented pick-and-place trajectories, the robustness against payload uncertainties of the proposed NMPC scheme was evaluated using the experiment illustrated in Figure 13. An additional payload of 15.1 kg was used, representing 65.6% of the mobile platform mass.

The obtained results are depicted in Figure 14. The same procedure was performed using the LMPC proposed in [28], leading to the comparison of Figure 15. Table II shows that, as for the results presented in Section VI-A1, substantially better tracking errors were obtained with the NMPC scheme.

TABLE II
SUMMARY OF COMPARATIVE ERRORS BETWEEN LMPC AND NMPC REGARDING THE ROBUSTNESS AGAINST PAYLOAD UNCERTAINTIES.

	RMS (SD)		Maximum error	
	TE	OE	TE	OE
LMPC	4.66 (3.46) mm	0.52 (0.40) °	12.37 mm	1.05°
NMPC	3.92 (2.82) mm	0.31 (0.23) °	7.83 mm	0.63°
Improvement	16.0 (18.3) %	40.7 (42.4) %	36.7%	40.0%

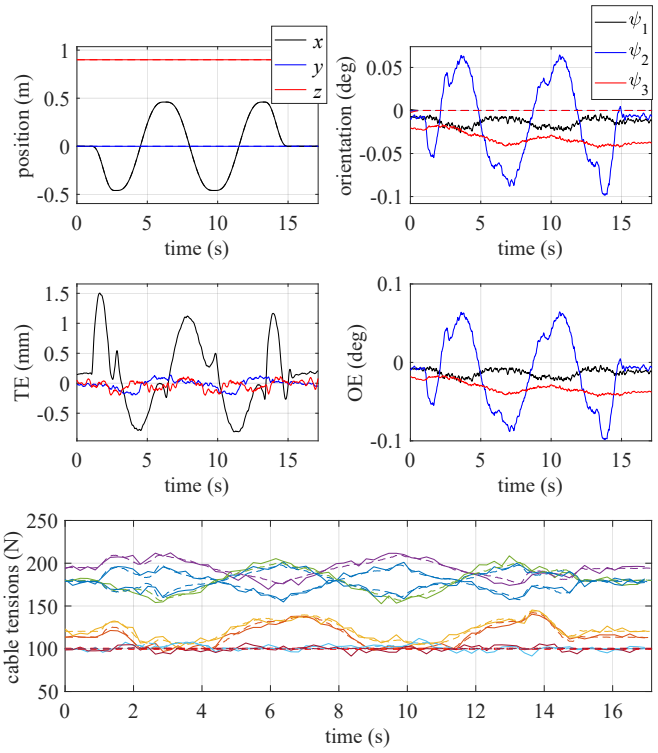

Fig. 16. High-speed trajectory results.

C. High-speed trajectory

As discussed in Section III, the proposed NMPC scheme considers that the cable tension control (block (d) in Figure 3) is able to maintain null errors all along the robot motion. This assumption combined to the long sampling period (22 ms) of the NMPC control loop could deteriorate the performance obtained for trajectories presenting high velocities and accelerations.

In order to evaluate whether the NMPC scheme is vulnerable to this issue, the trajectory depicted in Figure 16 was performed. The trajectory consists of two back and forth straight-line motions along the x direction with extreme poses 1.66 m away from each other. Maximum velocities and accelerations were equal to 0.915 m/s and 1.18 m/s^2, respectively. Regarding the positioning errors, the NMPC scheme led to maximum TE and OE equal to 2.06 mm and 0.138°, respectively. In contrast, the LMPC scheme results in maximum TE and OE of 7.32 mm and 0.210°. Hence, the NMPC scheme still performs better than the LMPC one in this experiment with velocities and accelerations larger than those in Sections VI-A1 and VI-A2.

Trajectories with higher velocities and accelerations might be successfully tracked by means of the proposed NMPC, but were not tested due to safety reasons since the HRPCable prototype was designed to handle heavy payloads at relatively limited velocities and accelerations. Nevertheless, the applicability of the proposed NMPC scheme to prototypes designed for high velocities and accelerations (such as [1], [67]) would require further investigations. This issue is mainly related to the computing time required to solve the OCP (16). On the one hand, a typical NMPC implementation would use numerical solvers implemented by experts (as discussed in [30]). This would reduce the computation time in comparison to the controller used in HRPCable, which was implemented from scratch. On the other hand, higher velocities and accelerations may lead to faster changes in the dynamic model (8). The solution of the optimization problem (16) may then demand a larger number of iterations of the numerical solver.

VII. CONCLUSIONS

This paper introduced an NMPC scheme for the position tracking of CDPRs. The OCP considered in the NMPC formulation handles explicitly the cable tensions and their limits. Accordingly, a substantial advantage of the proposed control scheme over typical state-of-the-art control strategies lies in its ability to operate on WFW boundary without failing. The proposed OCP formulation minimizes both the tracking error and the Wrench Equivalent Optimality (WEO). The latter is a non-negative measure able to evaluate whether the wrench generated by a given set of cable tensions can be generated by an alternative set with smaller 2-norm. The minimization of both the tracking error and the WEO is shown to be consistent, in the sense that a trajectory with minimal tracking error can be generated by cable tensions with minimal WEO. As a result, the stability of the closed-loop system can be analyzed and sufficient conditions for uniform asymptotic stability were deduced using tools for the analysis of NMPC schemes without terminal constraints and costs. Moreover, the proposed control scheme was validated experimentally on a 6-DoF CDPR driven by eight cables. In comparison to a previously introduced LMPC scheme, the tracking accuracy was substantially reduced.

While the experimental results showed that the proposed control scheme does not fail even in the presence of an unfeasible desired trajectory, the stability analysis presented in this paper is valid only for feasible trajectories. Future works may thus deal with the extension of the stability analysis of the proposed NMPC scheme to the case of unfeasible desired trajectories, aiming at obtaining the conditions under which the NMPC scheme remains stable while following a feasible trajectory as close as possible to the unfeasible desired one. Furthermore, the studied dynamic model considers that the inner control loop managing the cable tensions is able to generate the set of desired cable tensions instantly. Future works may consider, instead of (8), an augmented dynamical model taking into account the characteristics of this inner control loop. This approach may notably improve the vibration attenuation capabilities of the proposed NMPC scheme. Besides, a robustness analysis could evaluate the influence on the

stability of the closed-loop system of numerical and modeling errors involved in (8). Such an analysis may also consider the presence of measurement errors and disturbances.

APPENDIX A
DETAILS ON THE DYNAMIC MODELS

Neglecting cable sagging, the net wrench $\mathbf{f}(\boldsymbol{x},\boldsymbol{\tau}_c)$ applied on the platform by all the cable forces is

$$\mathbf{f}(\boldsymbol{x},\boldsymbol{\tau}_c) = \mathbf{W}(\boldsymbol{x})\,\boldsymbol{\tau}_c, \tag{58}$$

where the *wrench matrix* representing this linear mapping is given by $\mathbf{W}(\boldsymbol{x}) = -\mathbf{J}^T(\boldsymbol{x})$ with $\mathbf{J}(\boldsymbol{x})$ the Jacobian matrix (see [68]). Additionally, it is well-known that the angular velocity $\boldsymbol{\omega}$ is not equal to the time derivative of the orientation vector $\boldsymbol{\psi}$. Hence, the following relations need to be introduced:

$$\begin{aligned}\begin{bmatrix}\dot{\boldsymbol{p}}^T & \boldsymbol{\omega}^T\end{bmatrix}^T &= \mathbf{S}(\boldsymbol{x})\,\dot{\boldsymbol{x}}\\ \begin{bmatrix}\ddot{\boldsymbol{p}}^T & \dot{\boldsymbol{\omega}}^T\end{bmatrix}^T &= \mathbf{S}(\boldsymbol{x})\,\ddot{\boldsymbol{x}} + \dot{\mathbf{S}}(\boldsymbol{x},\dot{\boldsymbol{x}})\,\dot{\boldsymbol{x}},\end{aligned} \tag{59}$$

with $\mathbf{S}(\boldsymbol{x})$ a square matrix mapping $\dot{\boldsymbol{x}} = \begin{bmatrix}\dot{\boldsymbol{p}}^T & \dot{\boldsymbol{\psi}}^T\end{bmatrix}^T$ into $\begin{bmatrix}\dot{\boldsymbol{x}}^T & \boldsymbol{\omega}^T\end{bmatrix}^T$, and $\dot{\mathbf{S}}(\boldsymbol{x},\dot{\boldsymbol{x}})$ is the component-wise time derivative of $\mathbf{S}(\boldsymbol{x})$ (see for instance [69, Section 2.3] or [70, Section 3.6]).

The mobile platform equations of motion can be obtained with the Newton-Euler formalism, leading to the following dynamic model when the cable distributed mass is neglected:

$$\begin{aligned}\mathbf{M}'(\boldsymbol{x})\left(\dot{\mathbf{S}}(\dot{\boldsymbol{x}},\boldsymbol{x})\,\dot{\boldsymbol{x}} + \mathbf{S}(\boldsymbol{x})\,\ddot{\boldsymbol{x}}\right) + \mathbf{C}'(\dot{\boldsymbol{x}},\boldsymbol{x})\,\mathbf{S}(\boldsymbol{x})\dot{\boldsymbol{x}} = \\ \mathbf{g}(\boldsymbol{x}) + \mathbf{W}(\boldsymbol{x})\,\boldsymbol{\tau}_c,\end{aligned} \tag{60}$$

where matrices $\mathbf{M}'$ and $\mathbf{C}'$ are given by

$$\mathbf{M}'(\boldsymbol{x}) = \begin{bmatrix} m_p\,\mathbf{I} & -m_p\,\hat{\mathbf{c}}(\boldsymbol{x}) \\ m_p\,\hat{\mathbf{c}}(\boldsymbol{x}) & \mathbf{H}(\boldsymbol{x})\end{bmatrix} \text{ and} \tag{61}$$

$$\mathbf{C}'(\boldsymbol{x},\dot{\boldsymbol{x}})\,\dot{\boldsymbol{x}} = \begin{bmatrix} m_p\,\hat{\boldsymbol{\omega}}\,\hat{\boldsymbol{\omega}}\,\mathbf{c}(\boldsymbol{x}) \\ \hat{\boldsymbol{\omega}}\,\mathbf{H}(\boldsymbol{x})\,\boldsymbol{\omega}\end{bmatrix}. \tag{62}$$

The scalar m_p is the platform mass and $\mathbf{I}$ is an identity matrix with dimensions suitably chosen. For any pair of vectors $\mathbf{v}_1,\mathbf{v}_2 \in \mathbb{R}^3$, the matrix $\hat{\mathbf{v}}_1 \in \mathbb{R}^{3\times 3}$ represents the skew symmetric matrix such that $\hat{\mathbf{v}}_1\,\mathbf{v}_2 = \mathbf{v}_1 \times \mathbf{v}_2$, with $\times$ being the cross product. Denoting as $\mathbf{c}_p$ the position vector of the platform center of mass written in the coordinate system $\mathscr{O}_p$ attached to the platform (with $\mathscr{O}_p$ shown in Figure 2), the corresponding vector in the global coordinate system $\mathscr{O}_r$ is computed from $\mathbf{c}_p$ using the rotation matrix $\mathbf{R}(\boldsymbol{\psi})$ as follows:

$$\mathbf{c}(\boldsymbol{x}) = \mathbf{R}(\boldsymbol{\psi})\mathbf{c}_p = \begin{bmatrix} c_x & c_y & c_z\end{bmatrix}^T. \tag{63}$$

The angular velocity $\boldsymbol{\omega}$ is obtained from $\boldsymbol{x}$ and $\dot{\boldsymbol{x}}$ in accordance with (59). The matrix $\mathbf{H}$ is defined as $\mathbf{H}(\boldsymbol{x}) = \mathbf{R}(\boldsymbol{\psi})\,\mathbf{I}_G\,\mathbf{R}(\boldsymbol{\psi})^T + m_p\,\hat{\mathbf{c}}(\boldsymbol{x})\,\hat{\mathbf{c}}(\boldsymbol{x})^T$ where $\mathbf{I}_G$ is the platform inertia matrix with respect to the coordinate system $\mathscr{O}_p$. The vector of gravitational forces is $\mathbf{g}(\boldsymbol{x}) = m_p\,g\begin{bmatrix}0 & 0 & -1 & -c_y & c_x & 0\end{bmatrix}^T$, with g the gravitational acceleration. The z-axis of the fixed reference frame is assumed to be vertical directed upward. Additionally, denoting

$$\begin{aligned}\mathbf{M}(\boldsymbol{x}) &= \mathbf{M}'(\boldsymbol{x})\,\mathbf{S}(\boldsymbol{x}) \quad \text{and}\\ \mathbf{C}(\boldsymbol{x},\dot{\boldsymbol{x}}) &= \mathbf{C}'(\boldsymbol{x},\dot{\boldsymbol{x}})\,\mathbf{S}(\boldsymbol{x}) + \mathbf{M}'(\boldsymbol{x})\,\dot{\mathbf{S}}(\boldsymbol{x},\dot{\boldsymbol{x}}),\end{aligned} \tag{64}$$

the dynamic system (60) can be rewritten as

$$\mathbf{M}(\boldsymbol{x})\,\ddot{\boldsymbol{x}} + \mathbf{C}(\boldsymbol{x},\dot{\boldsymbol{x}})\,\dot{\boldsymbol{x}} = \mathbf{g}(\boldsymbol{x}) + \mathbf{W}(\boldsymbol{x})\,\boldsymbol{\tau}_c. \tag{65}$$

In order to define a discrete-time dynamic model based on (1), variables $\mathbf{x}_{k+1}$ and $\dot{\mathbf{x}}_{k+1}$ should be computed based on known $\mathbf{x}_k$, $\dot{\mathbf{x}}_k$ and $\boldsymbol{\tau}_k$. In accordance with (4), the cable tension vector $\boldsymbol{\tau}_k$ is considered as constant during a controller cycle period Δt. Therefore, the solutions $\boldsymbol{x}:\mathbb{R}\to\mathbb{R}^n$ and $\dot{\boldsymbol{x}}:\mathbb{R}\to\mathbb{R}^n$ of the Initial Value Problem (IVP) given by

$$\ddot{\boldsymbol{x}} = \mathbf{M}(\boldsymbol{x})^{-1}\left(\mathbf{g}(\boldsymbol{x}) + \mathbf{W}(\boldsymbol{x})\,\boldsymbol{\tau}_k - \mathbf{C}(\boldsymbol{x},\dot{\boldsymbol{x}})\,\dot{\boldsymbol{x}}\right), \tag{66a}$$

$$\boldsymbol{x}(t_k) = \mathbf{x}_k \text{ and } \dot{\boldsymbol{x}}(t_k) = \dot{\mathbf{x}}_k, \tag{66b}$$

lead to a transition mapping $\boldsymbol{\phi}_{\mathbf{x}}:\mathbb{R}^n\times\mathbb{R}^n\times\mathbb{R}^m\to\mathbb{R}^{2n}$ such that

$$\begin{bmatrix}\boldsymbol{x}(t_k+\Delta t)\\ \dot{\boldsymbol{x}}(t_k+\Delta t)\end{bmatrix} = \boldsymbol{\phi}_{\mathbf{x}}\left(\mathbf{x}_k,\dot{\mathbf{x}}_k,\boldsymbol{\tau}_k\right). \tag{67}$$

Using a more compact notation, the vector of the next state (pose and velocity)

$$\mathbf{y}_{k+1} = \begin{bmatrix}\boldsymbol{x}(t_k+\Delta t)^T & \dot{\boldsymbol{x}}(t_k+\Delta t)^T\end{bmatrix}^T \tag{68}$$

obtained with initial conditions

$$\begin{bmatrix}\boldsymbol{x}(t_k)^T & \dot{\boldsymbol{x}}(t_k)^T\end{bmatrix}^T = \mathbf{y}_k = \begin{bmatrix}\mathbf{x}_k^T & \dot{\mathbf{x}}_k^T\end{bmatrix}^T, \tag{69}$$

and application of constant cable tensions $\boldsymbol{\tau}_k \in \mathbb{R}^m$ is described with the transition mapping $\boldsymbol{\phi}_{\mathbf{y}}:\mathbb{R}^{2n}\times\mathbb{R}^m\to\mathbb{R}^{2n}$ according to

$$\mathbf{y}_{k+1} = \boldsymbol{\phi}_{\mathbf{y}}(\mathbf{y}_k,\boldsymbol{\tau}_k). \tag{70}$$

In general, the exact closed-form solution of the nonlinear IVP (66) cannot be determined. This IVP is solved with some numerical method (*e.g.* Euler or Runge-Kutta methods). It is also known that a numerical solution of (66) can be computed with an arbitrarily small error (according to the convergence theory of ordinary differential equations [71, Chapter 4]). In the present work, the numerical solution of the IVP (66) using the Euler method is considered. Accordingly, the discrete-time form of the state-space representation of the dynamic model (1) is approximated by (7). This rather simple solution is discussed in the remainder of this appendix.

Consider an instant $t_k = k\Delta t$, pose $\mathbf{x}_k \in \mathbb{R}^n$, velocity $\dot{\mathbf{x}}_k \in \mathbb{R}^n$ and cable tensions $\boldsymbol{\tau}_k \in \mathbb{R}^m$. The platform acceleration at the instant t_k is given by

$$\ddot{\boldsymbol{x}}(t_k) = \mathbf{M}(\mathbf{x}_k)^{-1}\left(\mathbf{W}(\mathbf{x}_k)\,\boldsymbol{\tau}_k + \mathbf{g}(\mathbf{x}_k) - \mathbf{C}(\mathbf{x}_k,\dot{\mathbf{x}}_k)\,\dot{\mathbf{x}}_k\right) = \ddot{\mathbf{x}}_k \tag{71}$$

The Euler integration method [71, Chapter 4] assumes the following approximation:

$$\begin{aligned}\boldsymbol{x}(t_k + k\,\Delta t) &= \boldsymbol{x}(t_k) + \dot{\boldsymbol{x}}(t_k)\,\Delta t\\ \dot{\boldsymbol{x}}(t_k + k\,\Delta t) &= \dot{\boldsymbol{x}}(t_k) + \ddot{\boldsymbol{x}}(t_k)\,\Delta t\end{aligned} \tag{72}$$

or, using the discrete counterparts of $\boldsymbol{x}$, $\dot{\boldsymbol{x}}$ and $\ddot{\boldsymbol{x}}$,

$$\begin{aligned}\mathbf{x}_{k+1} &= \mathbf{x}_k + \dot{\mathbf{x}}_k \Delta t \\ \dot{\mathbf{x}}_{k+1} &= \dot{\mathbf{x}}_k + \ddot{\mathbf{x}}_k \Delta t.\end{aligned} \tag{73}$$

The application of (71) in (73) leads to (7).

APPENDIX B
ON THE PROOF OF THEOREM 1

The results presented in [43, Chapter 6] are based on upper bounds of the cost functional. More precisely, these upper bounds are studied with respect to the *optimal value function*, which is defined in the following. For a $K \in \mathbb{N}$, the optimal value function $V_K : \mathbb{N} \times \mathbb{Y} \to \mathbb{R}$ is defined for an instant k and state $\mathbf{y}$ as follows:

$$\begin{aligned}V_K(k,\mathbf{y}) = \inf_{\boldsymbol{\tau}(\cdot)\in\mathbb{U}_k^K} & J_K\left(k,\mathbf{y},\boldsymbol{\tau}(\cdot)\right), \\ & \text{s.t. } \mathbf{y}_{\boldsymbol{\tau}(\cdot)}(j,\mathbf{y}) \in \mathbb{Y} \ \forall\, j \in \mathbb{N}_{1,K}\end{aligned} \tag{74}$$

with the cost functional J_K defined in (10). The scalar $V_K(k,\mathbf{y})$ is also known as the *cost-to-go* for given instant k and state $\mathbf{y}$ in the context of dynamic programming [72]. Note that, if the following optimal control problem possesses a global minimum

$$\begin{aligned}\boldsymbol{\tau}^*(\cdot) = \underset{\boldsymbol{\tau}(\cdot)\in\mathbb{U}_k^K}{\arg\min} & \sum_{j=0}^{K} \ell\big(k+j, \mathbf{y}_{\boldsymbol{\tau}(\cdot)}(j,\mathbf{y}), \boldsymbol{\tau}_{k+j}\big) \quad , \\ & \text{s.t. } \mathbf{y}_{\boldsymbol{\tau}(\cdot)}\big(j,\mathbf{y}\big) \in \mathbb{Y} \ \forall\ j \in \mathbb{N}_{1,K}\end{aligned} \tag{75}$$

then $\boldsymbol{\tau}^*(\cdot)$ satisfies

$$J_K\left(k,\mathbf{y},\boldsymbol{\tau}^*(\cdot)\right) = V_K(k,\mathbf{y}). \tag{76}$$

In order to deduce Theorem 1, let us first consider a simplified case with a constant desired state

$$\mathbf{y}_d(k) = \mathbf{y}_d \ \forall\ k \in \mathbb{N} \tag{77}$$

with a constant vector $\mathbf{y}_d \in \mathbb{Y}$. In this case, the closed-loop system is time invariant, the proposed NMPC scheme obtained with Algorithm 1 may be written as in [43, Algorithm 3.1] and the [43, Theorem 6.24] can be directly applied as it is. Moreover, the value function V_K is constant with respect to time and may be simplified to

$$V_K'(\mathbf{y}) = V_K(k,\mathbf{y}) \ \forall\ k \in \mathbb{N}. \tag{78}$$

Similarly, the stage cost and minimal stage cost can be simplified according to

$$\left.\begin{aligned}\ell_c(\mathbf{y},\boldsymbol{\tau}) &= \ell(k,\mathbf{y},\boldsymbol{\tau}) \\ \ell_c^*(\mathbf{y}) &= \ell^*(k,\mathbf{y})\end{aligned}\right\} \ \forall\ k \in \mathbb{N}. \tag{79}$$

The conditions for uniform asymptotic stability stated in [43, Theorem 6.24] addressing time-invariant systems are summarized as follows.

(i) There exist $\alpha_1, \alpha_2 \in \mathscr{K}_\infty$ such that for every $\mathbf{y} \in \mathbb{Y}$ the following inequalities hold:

$$\alpha_1(\|\mathbf{y}-\mathbf{y}_d\|) \leqslant \ell_c^*(\mathbf{y}) \leqslant \alpha_2(\|\mathbf{y}-\mathbf{y}_d\|); \tag{80a}$$

(ii) (*[43, Assumption 6.3] with linear B_K*) For each $\mathbf{y} \in \mathbb{Y}$ and $K \in \mathbb{N}$, there exists $\gamma_K \in \mathbb{R}$ with $\gamma_K < \infty$ so that the optimal cost functional $V_K'(\mathbf{y})$ satisfies

$$V_K'(\mathbf{y}) \leqslant \gamma_K\, \ell_c^*(\mathbf{y}). \tag{80b}$$

Additionally, [43, Lemma 6.6] shows that, if, for each $\mathbf{y} \in \mathbb{Y}$ and $N \in \mathbb{N}$, there exist $\boldsymbol{\tau}(\cdot) \in \mathbb{U}_0^N$ and real constants $C \geqslant 1$, $\sigma \in (0,1)$ such that

$$\ell_c\left(\mathbf{y}_{\boldsymbol{\tau}(\cdot)}(n,\mathbf{y}), \boldsymbol{\tau}_n\right) \leqslant C\,\sigma^n\, \ell_c^*(\mathbf{y}) \ \forall\ n \in \mathbb{N}_{1,N-1}, \tag{81}$$

then condition (80b) is satisfied with

$$\gamma_K = C\,\frac{1-\sigma^K}{1-\sigma} \tag{82}$$

and $\sup_K \gamma_K < \infty \ \forall\ K \in \mathbb{N}$.

Condition (81) is referred to as *exponential controllability*. Under this condition, there exists $\boldsymbol{\tau}(\cdot)$ that generates a trajectory with stage cost exponentially converging to zero in time.

Therefore, the conditions (80) are equivalently given as (80a) and (81). Considering (77) (and (79), consequently), the conditions of Theorem 1 are simplified to:

(a) There exist $\alpha_1, \alpha_2 \in \mathscr{K}\mathscr{L}_\infty$ such that

$$\alpha_1(\|\mathbf{y}-\mathbf{y}_d\|) \leqslant \ell_c^*(\mathbf{y}) \leqslant \alpha_2(\|\mathbf{y}-\mathbf{y}_d\|) \ \forall\ \mathbf{y} \in \mathbb{Y}. \tag{83}$$

(b) For all $\mathbf{y} \in \mathbb{Y}$, there exist feasible $\boldsymbol{\tau}^e(\cdot) \in \mathbb{S}^m$, real $C < \infty$ and $\sigma \in (0,1)$ satisfying

$$\ell_c\left(\mathbf{y}_{\boldsymbol{\tau}^e(\cdot)}(j,\mathbf{y}), \boldsymbol{\tau}_j^e\right) \leqslant C\,\sigma^j\, \ell_c^*(\mathbf{y}), \ \forall\ j \in \mathbb{N}. \tag{84}$$

These conditions are equivalent to (80a) and (81).

The time-varying case addressed in Theorem 1 is obtained considering [43, Assumptions 6.29 and 6.30], indicating that the results above can be straightforwardly extended to time-varying systems.

APPENDIX C
EXAMPLE OF TRIVIAL CONTROL LAW SATISFYING ASSUMPTION 1

Consider, for instance, a continuous-time control scheme that applies the wrench

$$\begin{aligned}\mathbf{f} = \mathbf{M}(\boldsymbol{x})\big(\ddot{\boldsymbol{x}}_d + \mathbf{K}_P(\boldsymbol{x}_d - \boldsymbol{x}) + \mathbf{K}_D(\dot{\boldsymbol{x}}_d - \boldsymbol{x})\big) + \\ + \mathbf{C}(\boldsymbol{x},\dot{\boldsymbol{x}})\,\dot{\boldsymbol{x}} - \mathbf{g}(\boldsymbol{x})\end{aligned} \tag{85}$$

with diagonal gain matrices $\mathbf{K}_P$ and $\mathbf{K}_D$. According to (1), the nominal closed-loop system dynamics is given by

$$\ddot{\boldsymbol{x}} = \ddot{\boldsymbol{x}}_d + \mathbf{K}_P(\boldsymbol{x}_d - \boldsymbol{x}) + \mathbf{K}_D(\dot{\boldsymbol{x}}_d - \boldsymbol{x}) \tag{86}$$

or, written in terms of the error $\boldsymbol{e}(t) = \boldsymbol{x}_d(t) - \boldsymbol{x}(t)$,

$$\ddot{\boldsymbol{e}} = -\mathbf{K}_D\,\dot{\boldsymbol{e}} - \mathbf{K}_P\,\boldsymbol{e}. \tag{87}$$

Choosing, for instance, $\mathbf{K}_P = \mathbf{K}_D = \mathbf{I}$, the solution to the differential equation (87) can be written as

$$\boldsymbol{e}(t) = e^{-t/2}\left(\mathbf{a}_1 \sin(\omega t) + \mathbf{a}_2 \cos(\omega t)\right), \tag{88}$$

with $\omega = \sqrt{3}/2$ and constant vectors $\mathbf{a}_1, \mathbf{a}_2 \in \mathbb{R}^n$ given by

$$\begin{aligned}\mathbf{a}_1 &= \boldsymbol{e}_0 \\ \mathbf{a}_2 &= \frac{1}{\omega}\left(\dot{\boldsymbol{e}}_0 - \frac{1}{2}\boldsymbol{e}_0\right)\end{aligned} \tag{89}$$

where $\boldsymbol{e}_0 = \boldsymbol{e}(0)$, $\dot{\boldsymbol{e}}_0 = \dot{\boldsymbol{e}}(0)$. The expressions of the error $\boldsymbol{e}$ and its time derivative satisfy

$$\begin{aligned}\|\boldsymbol{e}(t)\| = &\left\|e^{-t/2}\left(\mathbf{a}_1 \sin(\omega t) + \mathbf{a}_2 \cos(\omega t)\right)\right\| \leqslant \\ &\left(e^{-1/2}\right)^t \left(\|\mathbf{a}_1\| + \|\mathbf{a}_2\|\right)\end{aligned} \tag{90}$$

and

$$\begin{aligned}\|\dot{\boldsymbol{e}}(t)\| = &\left\|e^{-t/2}\mathbf{a}_3 \left(\sin(\omega t) + \mathbf{a}_4 \cos(\omega t)\right)\right\| \leqslant \\ &\left(e^{-1/2}\right)^t \left(\|\mathbf{a}_3\| + \|\mathbf{a}_4\|\right),\end{aligned} \tag{91}$$

with $\mathbf{a}_3 = \mathbf{a}_1/2 - \omega\,\mathbf{a}_2$ and $\mathbf{a}_4 = \mathbf{a}_2/2 + \omega\,\mathbf{a}_1$.

A tedious but straightforward computation using (89) leads to the bound $\|\boldsymbol{e}(t)\|^2 + \|\dot{\boldsymbol{e}}(t)\|^2 \leqslant c_{ey}\, e^{-t}\left(\|\boldsymbol{e}_0\|^2 + \|\dot{\boldsymbol{e}}_0\|^2\right)$, with $c_{ey} = (16 + 2\sqrt{3})/3$.

Consider $\mathbf{k}_{\mathbf{x}}, \mathbf{k}_{\dot{\mathbf{x}}} \in \mathbb{R}^n_+$, subvectors of $\mathbf{k}_{\mathbf{y}}$ (as in Section VI), and matrices $\mathbf{K}_{\mathbf{x}}, \mathbf{K}_{\dot{\mathbf{x}}} \in \mathbb{R}^{n\times n}$ diagonal matrices with $\mathbf{K}_{\mathbf{x}} = \operatorname{diag}(\mathbf{k}_{\mathbf{x}})$, $\mathbf{K}_{\dot{\mathbf{x}}} = \operatorname{diag}(\mathbf{k}_{\dot{\mathbf{x}}})$. Denoting also

$$K_{\mathbf{y}}^{max} = \max_i\left(k_{\mathbf{y},i}\right) \text{ and } K_{\mathbf{y}}^{min} = \min_i\left(k_{\mathbf{y},i}\right), \tag{92}$$

the following inequalities hold:

$$\begin{aligned}\|\boldsymbol{e}(t)\|^2_{\mathbf{K}_{\mathbf{x}}} + \|\dot{\boldsymbol{e}}(t)\|^2_{\mathbf{K}_{\dot{\mathbf{x}}}} &\leqslant K_{\mathbf{y}}^{max}\left(\|\boldsymbol{e}(t)\|^2 + \|\dot{\boldsymbol{e}}(t)\|^2\right) \\ &\leqslant \left(e^{-1}\right)^t K_{\mathbf{y}}^{max}\, c_{ey}\left(\|\boldsymbol{e}_0\|^2 + \|\dot{\boldsymbol{e}}_0^2\|\right) \\ &\leqslant \left(e^{-1}\right)^t \frac{K_{\mathbf{y}}^{max}}{K_{\mathbf{y}}^{min}}\, c_{ey}\left(\|\boldsymbol{e}_0\|^2_{\mathbf{K}_{\mathbf{x}}} + \|\dot{\boldsymbol{e}}_0\|^2_{\mathbf{K}_{\dot{\mathbf{x}}}}\right)\end{aligned}$$

which is the continuous counterpart of (29a) with $C_1 = c_{ey} K_{\mathbf{y}}^{max}/K_{\mathbf{y}}^{min} < \infty$ and $\sigma_1 = e^{-1} < 1$.

APPENDIX D
NUMERICAL SOLUTION OF THE OCP (16)

As discussed in Section VI, the presented experimental results were obtained with a control scheme implemented from scratch. Whereas the implementation of the basic mathematical operations are not noteworthy in this paper, the optimization techniques used in the solution of the OCP (16) deserves special attention. Since (16) is solved in real time, the implemented methods should combine good numerical accuracy and short computation time. The present section briefly discusses the optimization techniques used.

Besides the optimization problem corresponding to (16) itself, the solution of this OCP also includes the computation of the WEO, in accordance with (15). More precisely, the OCP obtained considering explicitly the upper (16) and lower (15) level optimization problems can be expressed as the bilevel minimization given by

$$\begin{aligned}\min_{\boldsymbol{\tau}(\cdot)\in\mathbb{U}_k^{h_p}} &\sum_{j=0}^{h_p-1} \|\mathbf{y}_{k+j} - \mathbf{y}_d(k+j)\|^2_{\mathbf{K}_{\mathbf{y}}} + \|\boldsymbol{\tau}_{k+j} - \boldsymbol{\tau}_{wo,k+j}\|^2_{\mathbf{K}_{\boldsymbol{\tau}}} \\ \text{s.t. } &\mathbf{y}_{k+j} = \begin{bmatrix}\mathbf{x}_{k+j}^T & \dot{\mathbf{x}}_{k+j}^T\end{bmatrix}^T = \mathbf{y}_{\boldsymbol{\tau}(\cdot)}\left(j, \mathbf{y}_k\right) \in \mathbb{Y}\ \forall\, j \in \mathbb{N}_{0,h_p} \\ &\boldsymbol{\tau}_{wo,k+j} = \arg\min_{\boldsymbol{\tau}'} \Big\{\|\boldsymbol{\tau}'\|^2 : \\ &\qquad \mathbf{W}(\mathbf{x}_{k+j})\,\boldsymbol{\tau}'_{k+j} = \mathbf{W}(\mathbf{x}_{k+j})\,\boldsymbol{\tau}_{k+j}, \\ &\qquad \boldsymbol{\tau}' \in \mathbb{U}\Big\}\ \forall\, j \in \mathbb{N}_{0,h_p-1}\end{aligned}$$

The present appendix discusses the numerical solution of both lower and upper level problems. Accordingly, Section D-A addresses the solution of (15) and Section D-B briefly describes the optimization strategy used in the solution of (16).

A. Computation of the WEO

The optimization problem (15) is a convex inequality constrained QP problem with non-empty feasible region (as discussed in the proof of Lemma 1). The results presented in Section VI were obtained with a control scheme that solves this optimization problem with an *active-set* method for convex QPs [73, Section 16.5]. More in detail, this method can determine the *exact* solution of the problem

$$\min_{\boldsymbol{\tau}}\ \boldsymbol{\tau}^T\boldsymbol{\tau} \tag{93a}$$

$$\text{s.t. } \mathbf{A}_{eq}\,\boldsymbol{\tau} = \mathbf{b}_{eq} \tag{93b}$$

$$\mathbf{A}_{ineq}\,\boldsymbol{\tau} \geqslant \mathbf{b}_{ineq} \tag{93c}$$

within a finite number of iterations. Matrices $\mathbf{A}_{ineq}$, $\mathbf{A}_{eq}$ and vectors $\mathbf{b}_{ineq}$, $\mathbf{b}_{eq}$ can be chosen so that constraints (93b)-(93c) are equivalent to (15b)-(15c), respectively. One may notably note that $\mathbf{A}_{eq} = \mathbf{W}(\mathbf{x})$. Each iteration consists of the solution of an equality constrained QP in which, besides (93b), some of the inequalities (93c) are taken as equalities and the remaining ones are neglected. More precisely, for an iteration $j \in \mathbb{N}$, the equality constrained QP

$$\begin{aligned}&\min_{\boldsymbol{\tau}}\ \boldsymbol{\tau}^T\boldsymbol{\tau} \\ &\text{s.t. } \mathbf{A}_j\,\boldsymbol{\tau} = \mathbf{b}_j\end{aligned} \tag{94}$$

is considered, where matrix $\mathbf{A}_j$ and vector $\mathbf{b}_j$ are given by

$$\mathbf{A}_j = \begin{bmatrix}\mathbf{A}_{eq} \\ \mathbf{A}'_{ineq,j}\end{bmatrix} \text{ and } \mathbf{b}_j = \begin{bmatrix}\mathbf{b}_{eq} \\ \mathbf{b}'_{ineq,j}\end{bmatrix} \tag{95}$$

with $\mathbf{A}'_{ineq,j}$ and $\mathbf{b}'_{ineq,j}$ composed of some of the rows of $\mathbf{A}_{ineq}$ and $\mathbf{b}_{ineq}$, respectively. The solution of (94) can be obtained finding the vectors of cable tensions $\boldsymbol{\tau}$ and of Lagrange multipliers $\boldsymbol{\mu}$ that satisfy the first-order optimality conditions (KKT conditions)

$$\begin{aligned}\boldsymbol{\tau} + \mathbf{A}_j^T\,\boldsymbol{\mu} &= \mathbf{0} \\ \mathbf{A}_j\,\boldsymbol{\tau} &= \mathbf{b}_j.\end{aligned} \tag{96}$$

The system of equations (96) can be solved straightforwardly applying the QR factorization [74, Section 5.2] of the matrix $\mathbf{A}_j^T$. This method can be particularly efficient since the QR factorization of $\mathbf{A}_{j+1}^T$ obtained in the iteration $j+1$ may be based on the factorization of $\mathbf{A}_j^T$ performed in the previous iteration. As detailed in [73, Section 16.5], matrices $\mathbf{A}_{j+1}$ and $\mathbf{A}_j^T$ differ at most of one row, and this similarity can be used in order to update the QR factorizations of successive iterations. Furthermore, one may note that the QR factorization of $\mathbf{A}_j^T$ is closely related to the computation of the null space of $\mathbf{W}(\mathbf{x})$, which is typically used in the existing state-of-the-art cable tension distribution algorithms.

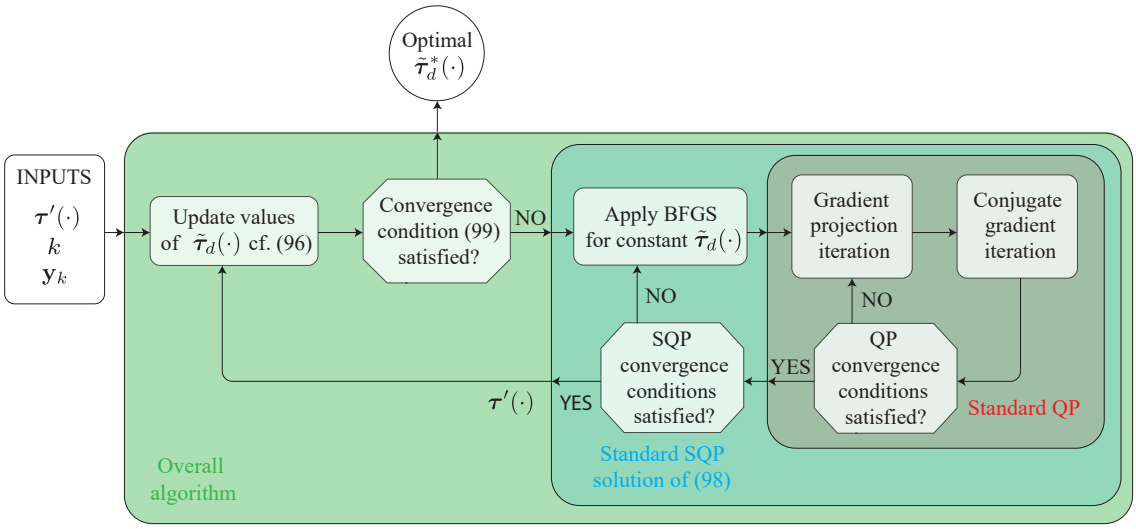

Fig. 17. Summary of the implemented numerical solution of the NPP corresponding to (16).

B. *Overall solution of* (16)

The implemented control scheme solves the OCP (16) applying *recursive elimination* (in accordance with [43, Section 12.1]). Therefore, the cost functional is computed with states $\mathbf{y}_{\boldsymbol{\tau}(\cdot)}(\cdot,\mathbf{y}_k)$ obtained by applying the transition mapping (8) recursively, as in (9). Alternative methods such as the *full discretization* and *multiple shooting* may also be used at the cost of increased dimension of the optimization problem. Details on these different approaches are discussed in [43, Section 12.1] and [33, Section 8.5].

The application of the recursive elimination leads to a Nonlinear Programming Problem (NPP) corresponding to the OCP (16). *Sequential Quadratic Programming* (SQP) and *interior-point* methods are often used to solve NPPs. The applicability of such algorithms in the implementation of NMPC controllers is studied in [43, Section 12.3] and [33, Section 8.7].

The use of an SQP algorithm is considered appropriate for the solution of the obtained NPP since the proposed OCP possesses a quadratic cost functional. Nocedal and Wright discuss the details of SQP methods in [73, Chapter 18]. These are iterative algorithms in which, at each iteration, the original nonlinear problem is approximated as a QP problem. A standard QP strategy may thus be used in the solution of each of these sub-problems.

In order to avoid the expensive computation of the second derivatives of the nonlinear cost function, a quasi-Newton BFGS approximation [73, Section 6.1] was used in the present work. This method estimates the Hessian of the cost function based on its first derivatives. While BFGS could be applied directly to the NPP obtained from (16), it has been observed that better performance is obtained with the optimization strategy summarized in Figure 17. Let $\boldsymbol{\tau}'(\cdot) \in \mathbb{U}_k^{h_p}$ be an initial guess for the optimal sequence of cable tensions at an instant $k \in \mathbb{N}$ and state $\mathbf{y}_k \in \mathbb{Y}$. The sequence $\tilde{\boldsymbol{\tau}}_d(\cdot)$ is defined as the WE-optimal tensions of $\boldsymbol{\tau}'(\cdot)$ given by

$$\tilde{\boldsymbol{\tau}}_d(k+j) = \boldsymbol{\tau}_{wo}(\mathbf{x}_{\mathbf{y}'(k+j)}, \boldsymbol{\tau}'_{k+j}),\ \forall\, j \in \mathbb{N}_{0,h_p-1} \tag{97a}$$

with $\mathbf{y}'(\cdot)$ the sequence of predicted states within the prediction horizon, obtained according to

$$\begin{aligned} \mathbf{y}'_k &= \mathbf{y}_k \\ \mathbf{y}'_{k+j+1} &= \boldsymbol{\phi}_{\mathbf{y}}(\mathbf{y}'_{k+j}, \boldsymbol{\tau}'_{k+j}),\ \forall\, j \in \mathbb{N}_{0,h_p-1}. \end{aligned} \tag{97b}$$

The WE-optimal tensions $\tilde{\boldsymbol{\tau}}_d(\cdot)$ in (97), which are computed with the method presented in Section D-A, are taken as reference to the cable tension optimization. Accordingly, one may define a simplified stage cost $\ell_{\tilde{\boldsymbol{\tau}}_d(\cdot)} : \mathbb{N} \times \mathbb{Y} \times \mathbb{U} \to \mathbb{R}$ given by

$$\ell_{\tilde{\boldsymbol{\tau}}_d(\cdot)}(k, \mathbf{y}, \boldsymbol{\tau}) = \|\mathbf{y} - \mathbf{y}_d(k)\|^2_{\mathbf{K}_\mathbf{y}} + \|\boldsymbol{\tau} - \tilde{\boldsymbol{\tau}}_d(k)\|^2_{\mathbf{K}_{\boldsymbol{\tau}}}. \tag{98}$$

The NPP corresponding to the stage cost $\ell_{\tilde{\boldsymbol{\tau}}_d(\cdot)}$ can be written as

$$\begin{aligned} \min_{\boldsymbol{\tau}(\cdot)}\ & \sum_{j=0}^{h_p-1} \ell_{\tilde{\boldsymbol{\tau}}_d(\cdot)}\left(k+j, y_{k+j}, \boldsymbol{\tau}_{k+j}\right) \\ \text{s.t. } & \mathbf{y}_{k+j+1} = \boldsymbol{\phi}_{\mathbf{y}}(\mathbf{y}_{k+j}, \boldsymbol{\tau}_{k+j}), \forall\, j \in \mathbb{N}_{0,h_p-1} \\ & \boldsymbol{\tau}(k+j) \in \mathbb{U}, \forall\, j \in \mathbb{N}_{0,h_p-1} \end{aligned} \tag{99}$$

A standard SQP algorithm is used in order to solve this NPP, resulting in an updated $\boldsymbol{\tau}'(\cdot)$ solution of (99) (as depicted in Figure 17). This procedure is applied iteratively for NPPs with updated $\tilde{\boldsymbol{\tau}}_d(\cdot)$, obtained according to (97). The overall algorithm is terminated once the difference between sequences $\tilde{\boldsymbol{\tau}}_d(\cdot)$ and $\boldsymbol{\tau}'(\cdot)$ is less than a given threshold. More precisely, the optimal sequence of cable tensions $\boldsymbol{\tau}_d^*(\cdot)$ is taken as $\boldsymbol{\tau}'(\cdot)$ when the following convergence condition is satisfied:

$$\sum_{j=0}^{h_p-1} \|\tilde{\boldsymbol{\tau}}_d(k+j) - \boldsymbol{\tau}'(k+j)\| \leqslant \varepsilon, \tag{100}$$

with a real positive ε, representing the desired convergence threshold. The optimal $\boldsymbol{\tau}_d^*(\cdot)$ is used as initial guess $\boldsymbol{\tau}'(\cdot)$ in the next sampling time $k+1$.

The implemented SQP algorithm applies the quasi-Newton BFGS estimation of the Hessian of (99). This estimation results in an inequality constrained QP problem. In accordance

with the case addressed in Section VI, the state constraint set is considered as $\mathbb{Y} = \mathbb{R}^{2n}$. Therefore, the QP inequality constraints consist uniquely of the cable tension limits, *i.e.*:

$$\boldsymbol{\tau}_{min} \leqslant \boldsymbol{\tau}_{k+j} \leqslant \boldsymbol{\tau}_{max}, \ \forall\, j \in \mathbb{N}_{0,h_p-1}. \tag{101}$$

One may note that the constraints (101) lead to a box constrained (or bound-constrained) QP. The *gradient projection* method [73, Section 16.7] is well known as an appropriate method for such QP problems. As illustrated in Figure 17, the proposed strategy couples the gradient projection with the *conjugate-gradient* method [73, Chapter 5] in order to obtain faster convergence. The implemented SQP algorithm can be classified as a *nonlinear gradient projection* method, briefly described in [73, Section 18.6].

REFERENCES

[1] S. Fang, D. Franitza, M. Torlo, F. Bekes, and M. Hiller, "Motion control of a tendon-based parallel manipulator using optimal tension distribution," *IEEE/ASME Transactions on Mechatronics*, vol. 9, no. 3, pp. 561–568, 2004.

[2] M. H. Korayem, H. Tourajizadeh, and M. Bamdad, "Dynamic load carrying capacity of flexible cable suspended robot: Robust feedback linearization control approach," *Journal of Intelligent and Robotic Systems: Theory and Applications*, vol. 60, no. 3-4, pp. 341–363, 2010.

[3] M. A. Khosravi and H. D. Taghirad, "Robust PID control of fully-constrained cable driven parallel robots," *Mechatronics*, vol. 24, no. 2, pp. 87–97, 2014.

[4] ——, "Dynamic modeling and control of parallel robots with elastic cables: Singular perturbation approach," *IEEE Transactions on Robotics*, vol. 30, no. 3, pp. 694–704, jun 2014.

[5] J. Lamaury and M. Gouttefarde, "Control of a Large Redundantly Actuated Cable-Suspended Parallel Robot," in *IEEE International Conference on Robotics and Automation*. IEEE, 2013, p. 211.

[6] J. Begey, L. Cuvillon, M. Lesellier, M. Gouttefarde, and J. Gangloff, "Dynamic Control of Parallel Robots Driven by Flexible Cables and Actuated by Position-Controlled Winches," *IEEE Transactions on Robotics*, vol. 35, no. 1, pp. 286–293, 2019.

[7] R. L. Williams, P. Gallina, and J. Vadia, "Planar translational cable-direct-driven robots," *Journal of Robotic Systems*, vol. 20, no. 3, pp. 107–120, 2003.

[8] A. Alikhani and M. Vali, "Sliding Mode Control of a Cable-driven Robot via Double-Integrator Sliding Surface," in *2012 International Conference on Control, Robotics, and Cybernetics*, 2012.

[9] R. Babaghasabha, M. A. Khosravi, and H. D. Taghirad, "Adaptive robust control of fully-constrained cable driven parallel robots," *Mechatronics*, vol. 25, no. 2, pp. 27–36, 2015.

[10] G. El-Ghazaly, M. Gouttefarde, and V. Creuze, "Adaptive terminal sliding mode control of a redundantly-actuated cable-driven parallel manipulator: CoGiRo," in *Cable-Driven Parallel Robots*, T. Bruckmann and A. Pott, Eds. Springer, 2015, vol. 32, pp. 179–200.

[11] C. Schenk, C. Masone, A. Pott, and H. H. Bülthoff, "Application of a differentiator-based adaptive super-twisting controller for a redundant cable-driven parallel robot," in *Cable-Driven Parallel Robots*, T. Bruckmann and A. Pott, Eds. Springer, 2018, vol. 53, pp. 254–267.

[12] M. H. Korayem, H. Tourajizadeh, M. Jalali, and E. Omidi, "Optimal path planning of spatial cable robot using optimal sliding mode control," *International Journal of Advanced Robotic Systems*, vol. 9, no. 5, p. 168, 2012.

[13] M. Zeinali and A. Khajepour, "Design and Application of Chattering-Free Sliding Mode Controller to Cable-Driven Parallel Robot Manipulator: Theory and Experiment," in *Volume 2: 34th Annual Mechanisms and Robotics Conference, Parts A and B*. ASME, jan 2010, pp. 319–327.

[14] S. R. Oh and S. K. Agrawal, "Nonlinear sliding mode control and feasible workspace analysis for a cable suspended robot with input constraints and disturbances," in *Proceedings of the 2004 American Control Conference*, vol. 5. IEEE, 2004, pp. 4631–4636.

[15] R. Chellal, L. Cuvillon, and E. Laroche, "Model identification and vision-based H-infinity position control of 6-DoF cable-driven parallel robots," *International Journal of Control*, vol. 90, no. 4, pp. 684–701, 2017.

[16] E. Laroche, R. Chellal, L. Cuvillon, and J. Gangloff, "A preliminary study for H infinity control of parallel cable-driven manipulators," in *Cable-Driven Parallel Robots*, T. Bruckmann and A. Pott, Eds. Springer, 2013, vol. 12, pp. 353–369.

[17] S. R. Oh and S. K. Agrawal, "Generation of feasible set points and control of a cable robot," *IEEE Transactions on Robotics*, vol. 22, no. 3, pp. 551–558, 2006.

[18] A. B. Alp and S. K. Agrawal, "Cable suspended robots: design, planning and control," in *Proceedings 2002 IEEE International Conference on Robotics and Automation (Cat. No.02CH37292)*, vol. 4. IEEE, 2002, pp. 4275–4280.

[19] J. J. Slotine, "Sliding controller design for non-linear systems," *International Journal of Control*, vol. 40, no. 2, pp. 421–434, 1984.

[20] S. Li and D. Zanotto, "Tracking control of fully-constrained cable-driven parallel robots using adaptive dynamic programming," in *Proc. IEEE/RSJ Int. Conf. Intelligent Robots and Systems (IROS)*, Macau, China, 2018, pp. 6781–6787.

[21] E. Ueland, T. Sauder, and R. Skjetne, "Optimal Force Allocation for Overconstrained Cable-Driven Parallel Robots: Continuously Differentiable Solutions With Assessment of Computational Efficiency," *IEEE Transactions on Robotics*, pp. 1–8, 2020.

[22] S. R. Oh and S. K. Agrawal, "Cable suspended planar robots with redundant cables: Controllers with positive tensions," in *IEEE Transactions on Robotics*, vol. 21, no. 3. IEEE, 2005, pp. 457–465.

[23] M. Gouttefarde, J. Lamaury, C. Reichert, and T. Bruckmann, "A Versatile Tension Distribution Algorithm for n-DOF Parallel Robots Driven by n + 2 Cables," *IEEE Transactions on Robotics*, vol. 31, no. 6, pp. 1444–1457, 2015.

[24] H. D. Taghirad and Y. B. Bedoustani, "An Analytic-Iterative Redundancy Resolution Scheme for Cable-Driven Redundant Parallel Manipulators," *IEEE Transactions on Robotics*, vol. 27, no. 6, pp. 1137–1143, dec 2011.

[25] C. Gosselin and M. Grenier, "On the determination of the force distribution in overconstrained cable-driven parallel mechanisms," *Meccanica*, vol. 46, no. 1, pp. 3–15, 2011.

[26] A. Pott, "An improved force distribution algorithm for over-constrained cable-driven parallel robots," in *Computational Kinematics*, F. Thomas and A. Perez Gracia, Eds., 2014, pp. 139–146.

[27] P. Bosscher, A. T. Riechel, and I. Ebert-Uphoff, "Wrench-feasible workspace generation for cable-driven robots," *IEEE Transactions on Robotics*, vol. 22, no. 5, pp. 890–902, 2006.

[28] J. C. Santos, A. Chemori, and M. Gouttefarde, "Redundancy Resolution integrated Model Predictive Control of CDPRs : Concept , Implementation and Experiments," in *Proceedings - IEEE International Conference on Robotics and Automation*, Paris, France, 2020, pp. 3889–3895.

[29] J. M. Maciejowski, *Predictive control: with constraints*. Pearson education, 2002.

[30] M. Katliar, J. Fischer, G. Frison, M. Diehl, H. Teufel, and H. H. Bülthoff, "Nonlinear Model Predictive Control of a Cable-Robot-Based Motion Simulator," *IFAC-PapersOnLine*, vol. 50, no. 1, pp. 9833–9839, 2017.

[31] R. Qi, M. Rushton, A. Khajepour, and W. W. Melek, "Decoupled modeling and model predictive control of a hybrid cable-driven robot (HCDR)," *Robotics and Autonomous Systems*, vol. 118, pp. 1–12, 2019.

[32] D. Q. Mayne, J. B. Rawlings, C. V. Rao, and P. O. M. Scokaert, "Constrained model predictive control: Stability and optimality," *Automatica*, vol. 36, no. 6, pp. 789–814, 2000.

[33] J. B. Rawlings, D. Q. Mayne, and M. M. Diehl, *Model predictive control: Theory, Computation, and Design*, 2nd ed. Santa Barbara, California: Nob Hill Pub., 2019.

[34] R. Chipalkatty, G. Droge, and M. B. Egerstedt, "Less Is More: Mixed-Initiative Model-Predictive Control With Human Inputs," *IEEE Transactions on Robotics*, vol. 29, no. 3, pp. 695–703, 2013.

[35] Z. Sun, Y. Xia, L. Dai, K. Liu, and D. Ma, "Disturbance Rejection MPC for Tracking of Wheeled Mobile Robot," *IEEE/ASME Transactions on Mechatronics*, vol. 22, no. 6, pp. 2576–2587, 2017.

[36] J. Nubert, J. Köhler, V. Berenz, F. Allgöwer, and S. Trimpe, "Safe and Fast Tracking on a Robot Manipulator: Robust MPC and Neural Network Control," *IEEE Robotics and Automation Letters*, vol. 5, no. 2, pp. 3050–3057, apr 2020.

[37] G. P. Incremona, A. Ferrara, and L. Magni, "MPC for Robot Manipulators With Integral Sliding Modes Generation," *IEEE/ASME Transactions on Mechatronics*, vol. 22, no. 3, pp. 1299–1307, jun 2017.

[38] T. Faulwasser and R. Findeisen, "Nonlinear Model Predictive Control for Constrained Output Path Following," *IEEE Transactions on Automatic Control*, vol. 61, no. 4, pp. 1026–1039, 2016.

[39] S. Heshmati-Alamdari, A. Eqtami, G. C. Karras, D. V. Dimarogonas, and K. J. Kyriakopoulos, "A self-triggered visual servoing model predictive control scheme for under-actuated underwater robotic vehicles," in *Proceedings - IEEE International Conference on Robotics and Automation*, may 2014, pp. 3826–3831.
[40] A. Boccia, L. Grüne, and K. Worthmann, "Stability and feasibility of state constrained MPC without stabilizing terminal constraints," *Systems & Control Letters*, vol. 72, pp. 14–21, 2014.
[41] L. Grüne, "NMPC without terminal constraints," *IFAC Proceedings Volumes*, vol. 45, no. 17, pp. 1–13, 2012.
[42] D. Mayne, "An apologia for stabilising terminal conditions in model predictive control," *International Journal of Control*, vol. 86, no. 11, pp. 2090–2095, nov 2013.
[43] L. Grüne and J. Pannek, "Nonlinear model predictive control," in *Nonlinear Model Predictive Control*. Springer, 2017.
[44] M. Khadem, J. O'Neill, Z. Mitros, L. da Cruz, and C. Bergeles, "Autonomous Steering of Concentric Tube Robots via Nonlinear Model Predictive Control," *IEEE Transactions on Robotics*, vol. 36, no. 5, pp. 1595–1602, 2020.
[45] J. R. Jurado Realpe, S. Abdelaziz, and P. Poignet, "Model Predictive Controller for a Planar Tensegrity Mechanism with Decoupled Position and Stiffness Control," in *Advances in Robot Kinematics*, J. Lenarčič and B. Siciliano, Eds. Cham: Springer International Publishing, 2021, pp. 349–358.
[46] J. C. L. Barreto, A. G. S. Conceição, C. E. T. Dórea, L. Martinez, and E. R. de Pieri, "Design and Implementation of Model-Predictive Control With Friction Compensation on an Omnidirectional Mobile Robot," *IEEE/ASME Transactions on Mechatronics*, vol. 19, no. 2, pp. 467–476, 2014.
[47] E. Kayacan, H. Ramon, and W. Saeys, "Robust Trajectory Tracking Error Model-Based Predictive Control for Unmanned Ground Vehicles," *IEEE/ASME Transactions on Mechatronics*, vol. 21, no. 2, pp. 806–814, 2016.
[48] A. Vivas and P. Poignet, "Predictive functional control of a parallel robot," *Control Engineering Practice*, vol. 13, no. 7, pp. 863–874, 2005.
[49] S. Wen, G. Qin, B. Zhang, H. K. Lam, Y. Zhao, and H. Wang, "The study of model predictive control algorithm based on the force/position control scheme of the 5-DOF redundant actuation parallel robot," *Robotics and Autonomous Systems*, vol. 79, pp. 12–25, 2016.
[50] K. Worthmann, M. W. Mehrez, M. Zanon, G. K. I. Mann, R. G. Gosine, and M. Diehl, "Model Predictive Control of Nonholonomic Mobile Robots Without Stabilizing Constraints and Costs," *IEEE Transactions on Control Systems Technology*, vol. 24, no. 4, pp. 1394–1406, jul 2016.
[51] H. K. Khalil, *Nonlinear control*. Pearson Higher Ed, 2015.
[52] L. Gagliardini, M. Gouttefarde, and S. Caro, "Determination of a Dynamic Feasible Workspace for Cable-Driven Parallel Robots," in *Advances in Robot Kinematics*, J. Lenarčič and J.-P. Merlet, Eds. Cham: Springer International Publishing, 2016, pp. 361–370.
[53] J. Eden, D. Lau, Y. Tan, and D. Oetomo, "Available acceleration set for the study of motion capabilities for cable-driven robots," *Mechanism and Machine Theory*, vol. 105, pp. 320–336, 2016.
[54] J. P. Merlet, "On the workspace of suspended cable-driven parallel robots," in *Proceedings - IEEE International Conference on Robotics and Automation*, vol. 2016-June. IEEE, 2016, pp. 841–846.
[55] M. Gouttefarde and C. Gosselin, "Analysis of the wrench-closure workspace of planar parallel cable-driven mechanisms," *IEEE Transactions on Robotics*, vol. 22, no. 3, pp. 434–445, 2006.
[56] A. Pott and W. Kraus, "Determination of the wrench-closure translational workspace in closed-form for cable-driven parallel robots," in *Proceedings - IEEE International Conference on Robotics and Automation*, vol. 2016-June. IEEE, 2016, pp. 882–887.
[57] J. C. Santos and M. Gouttefarde, "A Simple and Efficient Non-Model Based Cable Tension Control (in press)," in *Cable-Driven Parallel Robots*, T. Bruckmann and A. Pott, Eds. Springer, 2021.
[58] A. Pott and V. Schmidt, "On the forward kinematics of cable-driven parallel robots," in *2015 IEEE/RSJ International Conference on Intelligent Robots and Systems (IROS)*, 2015, pp. 3182–3187.
[59] J. Merlet, "A generic numerical continuation scheme for solving the direct kinematics of cable-driven parallel robot with deformable cables," in *2016 IEEE/RSJ International Conference on Intelligent Robots and Systems (IROS)*, 2016, pp. 4337–4343.
[60] J. C. Santos and M. Gouttefarde, "A Real-Time Capable Forward Kinematics Algorithm for Cable-Driven Parallel Robots Considering Pulley Kinematics," in *Advances in Robot Kinematics (ARK)*, 2020.
[61] S. Dempe, *Foundations of bilevel programming*, 1st ed. Springer Science & Business Media, 2002.
[62] W. Sun, G. Tang, and K. Hauser, "Fast UAV trajectory optimization using bilevel optimization with analytical gradients," *IEEE Transactions on Robotics*, vol. 37, no. 6, pp. 2010–2024, 2021.
[63] W. Shang, B. Zhang, B. Zhang, F. Zhang, and S. Cong, "Synchronization Control in the Cable Space for Cable-Driven Parallel Robots," *IEEE Transactions on Industrial Electronics*, vol. 66, no. 6, pp. 4544–4554, 2019.
[64] W. Shang, B. Zhang, S. Cong, and Y. Lou, "Dual-space adaptive synchronization control of redundantly-actuated cable-driven parallel robots," *Mechanism and Machine Theory*, vol. 152, p. 103954, 2020.
[65] J. C. Santos, A. Chemori, and M. Gouttefarde, "Model Predictive Control Applied to Large-Dimension Cable-Driven Parallel Robots," in *Cable-driven parallel robots*, 2019.
[66] Beckhoff, *TwinCAT 3 - C++ Manual*, 1st ed. Beckhoff, 2019.
[67] S. Kawamura, W. Choe, S. Tanaka, and S. R. Pandian, "Development of an ultrahigh speed robot FALCON using wire drive system," *Proceedings - IEEE International Conference on Robotics and Automation*, vol. 1, no. 1, pp. 215–220, 1995.
[68] T. Bruckmann, L. Mikelsons, T. Brandt, M. Hiller, and D. Schramm, "Wire Robots Part I: Kinematics, Analysis & Design," in *Parallel Manipulators, New Developments*. InTech, 2008, vol. 1, pp. 109–132.
[69] P. C. Hughes, *Spacecraft attitude dynamics*. Dover Publications, 2004.
[70] B. Siciliano, L. Sciavicco, L. Villani, and G. Oriolo, *Robotics: Modelling, Planning and Control*. Springer-Verlag London Limited, 2009, no. 4.
[71] P. Deuflhard and F. Bornemann, *Scientific Computing with Ordinary Differential Equations*, 1st ed. New York: Springer-Verlag New York, 2002.
[72] D. P. Bertsekas, *Dynamic Programming and Optimal Control*, 3rd ed. Nashua, USA: Athena Scientiific, 2005.
[73] J. Nocedal and S. Wright, *Numerical optimization*. Springer Science and Business Media, 2006.
[74] G. H. Golub and C. F. Van Loan, "Matrix computations, Fourth Edition," 2013.

João Cavalcanti Santos received the B.Eng. and M.Sc. degrees in mechanical engineering from the University of São Paulo, São Carlos, Brazil, in 2015 and 2017, respectively, and the Ph.D. degree in robotics from the LIRMM, Montpellier, France, in 2020, working in the European H2020 project Hephaestus.
He is currently a Postdoctoral Fellow with INSERM, Montpellier. His main research interests include robot design and control, numerical optimization, and model predictive control.

Marc Gouttefarde (Member IEEE) received the B.Eng. degree in mechatronics from Institut National des Sciences Appliquées, Strasbourg, France, in 2001, and the M.Sc. and Ph.D. degrees in mechanical engineering from Laval University, Québec, QC, Canada, in 2002 and 2005, respectively.
From 2005 to 2007, he was a Postdoctoral Fellow with INRIA, Sophia-Antipolis, France. He is currently a CNRS Senior Researcher with LIRMM, Montpellier, France, where he is mainly working on the design, control, and applications of cable-driven parallel robots. Dr. Gouttefarde is currently the head of LIRMM Robotics Department and an Associate Editor for the IEEE Transactions on Robotics.

Ahmed Chemori (Senior Member IEEE) received the M.Sc. and Ph.D. degrees both in automatic control from the Grenoble Institute of Technology, Grenoble, France, in 2001 and 2005, respectively. He has been a Postdoctoral Fellow with the Automatic Control Laboratory, Grenoble, France, in 2006. He is currently a tenured Research Scientist in automatic control and robotics with the Montpellier Laboratory of Informatics, Robotics, and Microelectronics (LIRMM). His research interests include nonlinear, adaptive, robust and predictive control and their applications in robotics.